RESEARCH ARTICLE

A cortical–hippocampal communication undergoes rebalancing after new learning

Arron F Hall, Dong V Wang*

Department of Neurobiology and Anatomy, Drexel University College of Medicine, Philadelphia, United States

eLife Assessment

This **valuable** study investigates communication from the anterior cingulate cortex to the hippocampus during learning. The optogenetic evidence supporting the functional connection, including the interneurons likely to be involved, is **convincing**. However, the evidence linking this pathway to learning and memory and certain aspects of the statistical interpretation remains limited. Overall, the work will be of interest to neuroscientists studying cortical–hippocampal interactions and learning and memory.

Abstract The brain's ability to consolidate a wide range of memories while maintaining their distinctiveness across experiences remains poorly understood. Sharp-wave ripples, neural oscillations that occur predominantly within CA1 of the hippocampus during immobility and sleep, have been shown to play a critical role in the consolidation process. More recently, evidence has uncovered functional heterogeneity of pyramidal neurons within distinct sublayers of CA1 that display unique properties during ripples, potentially contributing to memory specificity. Despite this, it remains unclear exactly how ripples shift the activity of CA1 neuronal populations to accommodate the consolidation of specific memories and how sublayer differences manifest. Here, we studied interactions between the anterior cingulate cortex (ACC) and CA1 neurons during ripples and discovered a reorganization of their communication following learning. Specifically, using a generalized linear model decoder, we demonstrated the pre-existence of ACC-to-CA1 communication, which is weakened during post-training sleep following learning, suggesting that ACC activity reallocates the contribution of CA1 neurons during memory formation. Interestingly, the reorganization appeared unique for a subset of CA1 superficial (CA1sup) neurons that were task inactive, whereas communication between the ACC and CA1deep neurons remained largely stable across pre- and post-training sleep. Consistent with this sublayer-selective reorganization, we found that optogenetic stimulations of the ACC preferentially suppressed CA1sup neurons while activating a unique subset of CA1 interneurons. Overall, these findings highlight an important role of the ACC in rebalancing CA1 neuronal populations' contribution in learning and memory consolidation.

***For correspondence:** dw657@drexel.edu

Competing interest: See page 17

Funding: See page 17

Preprint posted
29 March 2025
Sent for Review
30 April 2025
Reviewed preprint v1
14 July 2025
Reviewed preprint v2
16 September 2026
Version of Record
01 October 2026

Reviewing Editor: Adrien Peyrache, McGill University, Canada

© Copyright Hall and Wang. This article is distributed under the terms of the Creative Commons Attribution License, which permits unrestricted use and redistribution provided that the original author and source are credited.

Introduction

Memories are not static; rather, they are gradually consolidated into long-term traces across days, weeks, or longer (***Klinzing et al., 2019***; ***Squire et al., 2015***). At any given moment, we are processing and consolidating an array of differing experiences. The ability to preserve distinctiveness across these various experiences is essential for memory consolidation. This requires a delicate balance between the mechanisms that facilitate the reactivation and transformation of new memories alongside those that regulate consolidation to prevent the intermingling of distinct experiences. While much attention has been focused on uncovering the principles that guide the reactivation and consolidation of

memories, less is known about the mechanisms that regulate these processes and govern memory specificity.

During sleep, sharp-wave ripples, neural oscillations predominantly within the CA1 of the hippocampus, facilitate hippocampal reactivations and accompany cortical reactivations of memory-related neurons, a process referred to as replay (***Buzsáki, 2015***; ***Buzsáki et al., 1992***; ***Davidson et al., 2009***; ***Diba and Buzsáki, 2007***; ***Foster and Wilson, 2006***; ***Lee and Wilson, 2002***). Replay has been shown to be essential for memory consolidation as disruption or enhancement of ripples impairs or improves memory, respectively (***Ego-Stengel and Wilson, 2010***; ***Fernández-Ruiz et al., 2019***; ***Girardeau et al., 2009***; ***Gridchyn et al., 2020***; ***Jadhav et al., 2012***; ***Wang et al., 2015***). Recently, evidence has uncovered functional and anatomical heterogeneity in CA1 neurons based on their position within the pyramidal layer: the superficial (CA1sup) and deep (CA1deep) sublayers (***Danielson et al., 2016***; ***Geiller et al., 2017***; ***Hall and Wang, 2023***; ***Harvey et al., 2023***; ***Mizuseki et al., 2011***; ***Sharif et al., 2021***). CA1sup neurons have more stable firing rates and higher spatial acuity (***Danielson et al., 2016***; ***Harvey et al., 2023***; ***Mizuseki et al., 2011***), whereas CA1deep neurons respond more to enriched environments, sensory landmarks, and reward (***Danielson et al., 2016***; ***Geiller et al., 2017***; ***Harvey et al., 2023***; ***Sharif et al., 2021***). During replay events, CA1sup neurons show increased activity after spatial learning, whereas CA1deep neurons show decreased activity (***Berndt et al., 2023***; ***Harvey et al., 2023***). Together, ripples and the recruitment of distinct subpopulations within CA1 drive new memory formation. Despite this understanding, the mechanisms that regulate their activity to balance consolidation across experiences remain unclear.

Emerging evidence has demonstrated the importance of suppression within the hippocampal network to balance neuronal excitability surrounding learning (***Gava et al., 2024***; ***Karaba et al., 2024***; ***Norimoto et al., 2018***). During pre-learning sleep, ripples depotentiate synapses that, if perturbed, impair learning (***Norimoto et al., 2018***). Similarly, after learning, ripples facilitate the depotentiation of memory-unrelated neurons (***Norimoto et al., 2018***). Additionally, during post-learning sleep, hippocampal neurons initially display heightened firing rates before ultimately returning to baseline (***Giri et al., 2019***; ***Wilson and McNaughton, 1994***). Prior studies have demonstrated that reestablishing baseline is necessary for learning, as excessive neuronal activity and synchrony impairs learning (***Gava et al., 2024***; ***Karaba et al., 2024***). Suppression of the hippocampus, then, appears to play a key role in down-regulating synapses, preventing memory saturation, and promoting memory flexibility (***Balduzzi and Tononi, 2013***). Interestingly, CA1sup neurons appear to be the most sensitive to this process (***Gava et al., 2024***). Following repetitive learning, CA1sup neurons become highly synchronized and coactive, which impairs future memory formation (***Gava et al., 2024***). Correspondingly, optogenetic inhibition of CA1sup, but not CA1deep neurons, after learning decouples and decreases neuronal activity, which reduces rigidity and restores new memory formation (***Gava et al., 2024***). Still, exactly how facilitation and suppression are balanced throughout consolidation, and whether cortical inputs play a role in modifying hippocampal activity in this process, remains poorly understood.

Here, we employ in vivo electrophysiology recording across contextual fear conditioning (CFC) and sleep to understand how communication between the anterior cingulate cortex (ACC) and hippocampal CA1 are modified following learning. Previous studies have shown that the ACC displays increased activity immediately preceding CA1 ripples and is instrumental in CFC and memory consolidation (***Einarsson and Nader, 2012***; ***Frankland et al., 2004***; ***Wang and Ikemoto, 2016***). We uncovered a novel, sublayer-specific, line of communication between ACC and CA1 surrounding ripples, with ACC preferentially communicating with CA1sup neurons. This communication rebalances following learning, suggesting a potential role in memory consolidation.

Results

Pre-ripple ACC activity predicts CA1 activity during ripples

To understand how the ACC and hippocampus communicate surrounding learning, we employed simultaneous dual-site in vivo electrophysiology recordings of both regions throughout a CFC paradigm (***Figure 1A and B***). In this approach, we were able to examine ACC–CA1 communication prior to, during, and after learning, enabling us to examine how this communication evolves across fear learning. Specifically, we emphasized investigation into communication changes between pre- and post-training sleep to understand whether functional connectivity undergoes learning-related

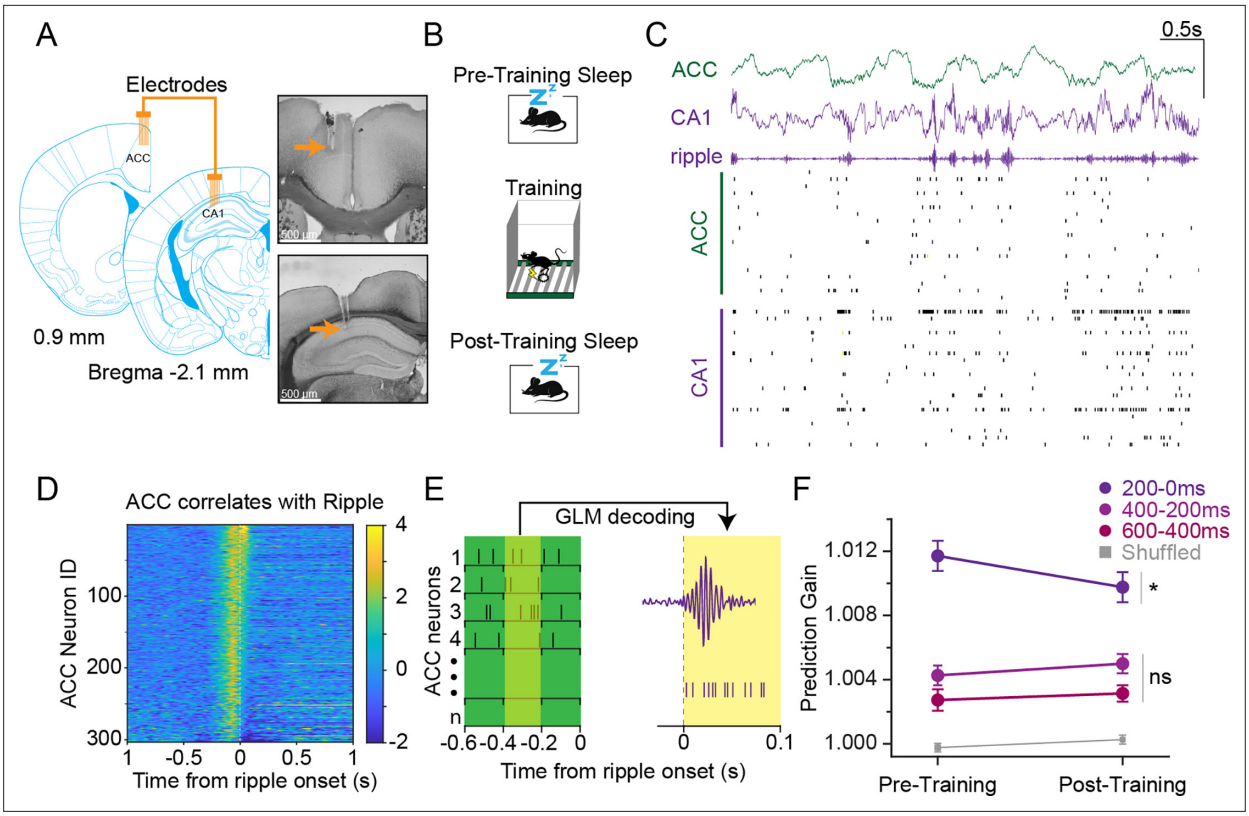


Figure 1. Pre-ripple ACC activity predicts CA1 activity during ripples. (**A**) Left: schematic of a dual 8-tetrode array implanted in the ACC and CA1. Right: two representative brain sections highlighting the recording sites (orange arrows) in the ACC and CA1, top and bottom, respectively. (**B**) Schematic of the contextual fear memory procedure. (**C**) Top: representative ACC and CA1 LFP from a pre-training sleep session, Y axis scale bar 1 mV. Bottom: individual spikes across ACC and CA1 neurons. (**D**) Heatmap of ACC neuron (N=10 animals; N=303 neurons) activity during pre-training sleep surrounding ripple onsets (bin = 5 ms). (**E**) Schematic of GLM decoder. 200 ms bins of ACC spiking data preceding ripple predict CA1 activity 0–100 ms after ripple onset. (**F**) Prediction gain difference in decoding CA1 activity between real and shuffled ACC activity across three pre-ripple predictor windows (–200 to 0 ms, –400 to –200 ms, and –600 to –400 ms; N=10 animals; N=291 CA1 neurons). Repeated measures mixed-model analysis revealed a significant effect of predictor type, with real prediction gain exceeding shuffled prediction gain overall ($p<0.001$), and a significant effect of predictor window ($p<0.001$). There was also a significant effect of session (pre vs post) on prediction gain that varied across predictor windows (Window ×session interaction, $p=0.010$). Post hoc comparisons showed that prediction gain was highest in the –200 to 0 ms window relative to earlier windows during pre- and post-training sleep (all Holm-corrected, $p<0.001$). Additionally, the –200 to 0 ms window exhibited a significant pre-to-post decrease in prediction gain (Wilcoxon signed-rank, $p=0.022$), whereas the other windows did not. Error bars indicate ± SEM.

The online version of this article includes the following figure supplement(s) for figure 1:

Figure supplement 1. ACC→CA1 coupling decreases for CA1sup neurons.

Figure supplement 2. Prediction gain differences per animal.

reorganization. Local field potentials (LFPs) and neuronal spikes were recorded simultaneously, and slow-wave sleep was identified by CA1 delta-to-theta power ratio and the animal's immobility (***Figure 1C***; ***Wang et al., 2015***).

We first examined ACC neuronal spiking activity surrounding CA1 ripples during pre-training sleep. Across 10 mice, we recorded 303 ACC neurons, with individual counts per animal ranging between 19 and 48 neurons. Most ACC neurons (235/303) displayed significant changes in activity surrounding ripples compared to baseline (***Figure 1D***; see 'Methods'). Of the neurons with significant changes, the majority displayed a pre-ripple activation (81.7%; 192/235) while a minority (18.3%; 43/235) showed a more prominent post-ripple activation (***Figure 1D***). To determine whether this coordinated activity is indicative of information flow, we implemented general linear model (GLM) machine learning decoding to test whether population ACC activity preceding ripples can predict CA1 activity during ripples (***Figure 1E***; ***Liu et al., 2024b***; ***Rothschild et al., 2017***). ACC spiking was binned into 200 ms segments across multiple time windows to predict individual CA1 neuronal firing rates between 0 and 100 ms after ripple onset (***Figure 1E***; see 'Methods'). The decoder was trained on 50% of the recorded

data upon which the remaining 50% data was used for testing. All GLM decoding was performed on spike data recorded during slow-wave sleep epochs before or after training. We found that across multiple time-windows, prediction gain (PG) score using real data was significantly higher than shuffled (***Figure 1F***). PG score was greatest when using ACC spiking –200 to 0 ms preceding ripple onset, aligning with the observed correlated firing seen in ***Figure 1D***. Moreover, only this window showed learning-related changes with a significant decrease in PG score in post-training sleep. In accordance, all subsequent GLM analyses in this paper will use the –200 to 0 ms time window (***Figure 1F***).

Our GLM analysis generated a PG score for each CA1 neuron, enabling us to examine how PG scores correlate and shift with other properties of CA1 neurons. We first asked whether the learning-related reduction in PG score reflected a global dampening of ACC→CA1 communication or a selective redistribution across CA1 neurons. To test this, we examined the stability of PG scores between pre- and post-training sleep. Preservation of PG score ranking among CA1 neurons would suggest that learning weakens existing ACC→CA1 communication while maintaining the relative contribution of individual ACC neurons, consistent with a global dampening effect. In contrast, poor preservation of PG score ranking would be more indicative of a reorganization of ACC→CA1 communication. We found that PG scores were positively correlated across sessions, that is, CA1 neurons with high PG scores before learning tended to retain relatively high PG score after learning (***Figure 2A***). To further assess the stability of PG score ranking, we performed permutation-based preservation analyses (***Figure 2B***). Neurons in the top PG score quartile were significantly more likely than expected by chance to remain in the top quartile following learning, whereas transitions between top and bottom quartiles were rare. Together, these findings suggest that functional connectivity between the ACC and CA1 is broadly dampened after learning rather than undergoing robust reorganization.

To examine ACC–CA1 communication independently of the GLM analysis, we computed spike-triggered averages (STA) of CA1 neuron activity using a pooled ACC spike train generated by merging spikes from all recorded ACC neurons. We performed a full lag-resolved analysis in which CA1 spike trains were aligned to ACC spike times, baseline-normalized, and quantified in 10 ms bins across a peri-ACC-spike window (***Figure 1—figure supplement 1A and B***). This analysis revealed a significant reduction in CA1 activity following ACC population spiking in post- compared to pre-training sleep, suggesting a reduction in ACC–CA1 coupling after learning, consistent with the GLM decoding results.

Task-inactive CA1 neurons reshape their activity with ACC after learning

Since overall functional connectivity between ACC and CA1 changed after learning, we next asked whether PG scores across CA1 neurons differed based on their activity during training. To test this, we calculated a modulation index by comparing each CA1 neurons' firing rate during training with its pre-training baseline (***Figure 2C***; ***Karaba et al., 2024***). We found that predication gain change (ΔPG) showed a modest positive correlation with modulation index, indicating that task engagement modifies ACC→CA1 communication (***Figure 2C***). To investigate this relationship further, CA1 neurons were separated into modulation-index quartiles and their ΔPG were compared across quartiles. Although the overall effect of quartile did not reach significance in the linear mixed-effects model, neurons in the bottom quartile (task-inactive) exhibited a significant reduction in ΔPG, whereas no significant changes were observed in the remaining quartiles (***Figure 2D***). To better illustrate this effect, we next compared pre- and post-training PG scores in the top and bottom quartiles. Consistent with the ΔPG analysis, only neurons in the bottom quartile exhibited a significant reduction in PG scores following learning, suggesting that the learning-related decreases in ACC→CA1 communication are primarily driven by a loss in functional connectivity with bottom-quartile CA1 neurons (task-inactive) (***Figure 2E***). Lastly, we examined whether PG scores correlated with the freezing response in mice during recall. Across all mice, freezing was significantly higher during recall than pre-shock baseline during training (***Figure 2—figure supplement 1A***). Overall, we found no correlation between PG and freezing (***Figure 2—figure supplement 1B–D***). However, there was a trend for a positive correlation ($p=0.07$) between ΔPG and freezing percentage. An important consideration is that the uniformly high levels of freezing in mice limited behavioral variability, potentially reducing our ability to detect relationships between ACC–CA1 communication decoding and behavioral differences.

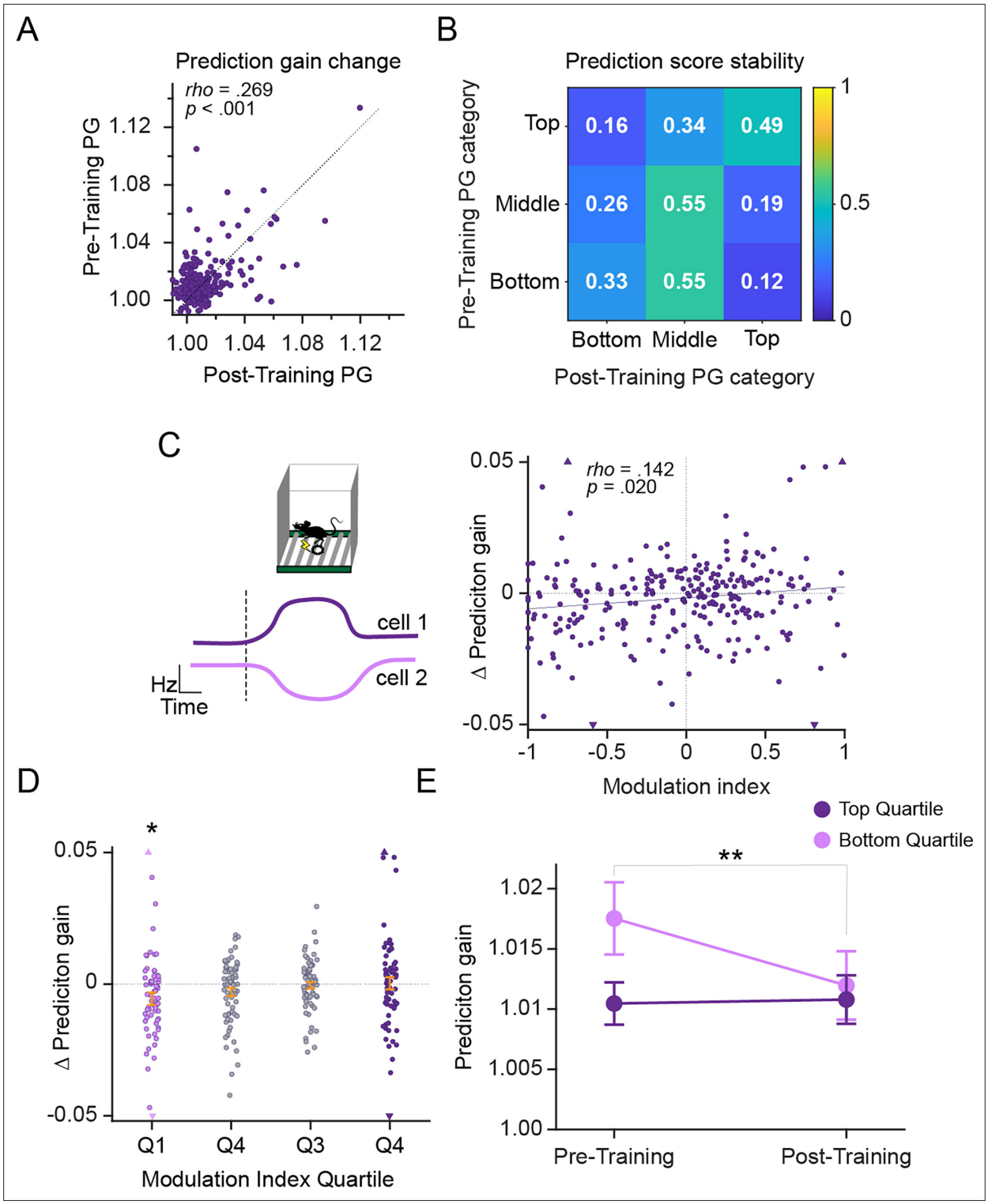


Figure 2. Learning dampens ACC→CA1 communication, which differs based on task engagement. (**A**) Correlation of PG scores between pre- and post-training sleep (N=10 animals; N=291 CA1 neurons). Spearman's rho revealed a significant correlation between pre- and post-training sleep, rho = 0.269 p<0.001. (**B**) PG score rank preservation permutation matrices. Permutation testing revealed that nearly half of CA1 neurons in the top PG score quartile remained in the top quartile after training (49.3%, permutation p<0.001), significantly exceeding chance expectations. Whereas retention of bottom-quartile neurons was weaker, showing only a trend above chance (32.9%, permutation p=0.052). Extreme transitions between top and bottom categories were uncommon and not enriched above chance (p=0.999). (**C**) Left: schematic of two representative neurons' firing patterns during training. Neuron 1 increases and Neuron 2 decreases activity during training. Right: correlation scatter plot of CA1 neuron ΔPG and modulation index.

Figure 2 continued on next page

Figure 2 continued

Spearman's rho revealed a modest positive correlation between variables, rho = 0.142, p=0.020. Purple triangles indicate extreme values that were included in all statistical analyses but are cropped for visualization purposes. (**D**) ΔPG as a function of modulation index quartiles (N=66 per quartile). Overall quartile effect did not reach significance (Kruskal–Wallis, p=0.081). (**E**) PG scores as a function of task modulation. Neurons were divided into the top and bottom modulation index (MI) quartiles. A linear mixed-effects model revealed significant effects of MI quartile (p=0.005) and session (p=0.017), with a trend-level MI quartile × session interaction (p=0.074). Post hoc comparisons showed a significant pre-to-post reduction in PG score for neurons in the bottom MI quartile (Holm-corrected, p=0.010), whereas neurons in the highest MI quartile showed no significant change (Holm-corrected, p=0.831). Error bars indicate ± SEM.

The online version of this article includes the following figure supplement(s) for figure 2:

Figure supplement 1. CFC freezing response correlated with prediction gain (PG).

Figure supplement 2. Modulation index changes across CFC and modulation index differences between sublayers.

ACC displays a distinct relationship with CA1 sublayers

It has been well established that functional heterogeneity exists within the pyramidal layer of CA1 (***Hall and Wang, 2023***; ***Mizuseki et al., 2011***). To investigate whether ACC communication is different across CA1 sublayers, we separated CA1 neurons into CA1sup and CA1deep neurons based on their sharp-wave deflection characteristics (***Figure 3A***; for details see 'Methods'; ***Danielson et al., 2016***; ***Mizuseki et al., 2011***). We first asked whether CA1 sublayers displayed differences in GLM decoding after learning. Although PG score was significantly higher for each sublayer compared to shuffled, neither sublayer showed a learning-related difference (trend p=0.058), nor was there a significant difference between sublayers (***Figure 3B***). While GLM decoding revealed similar PG scores across CA1 sublayers, it remains possible that the stability of the predictive relationship differed between them. Therefore, we examined how well PG scores correlated between pre- and post-training sleep and the degree of retention for the highly predicted neurons. Our results show that CA1sup neurons showed no significant correlation in PG scores across sessions, and permutation testing revealed that the highly predicted neurons were not retained above chance levels (***Figure 3C and D***). In contrast, CA1deep neurons exhibited significant PG score preservation across sessions, with both positive pre-to-post correlations and above-chance retention for the highly predicted neurons (***Figure 3E and F***). Together, these results suggest that ACC→CA1sup communication is more dynamic and evolving across learning, whereas ACC→CA1deep communication remains comparatively stable.

Given the differences in PG score stability across CA1 sublayers, we next asked whether task engagement further influenced ACC→CA1 sublayer connectivity. We first examined whether ΔPG correlated with modulation index. In CA1sup neurons, we found a significant correlation between ΔPG and modulation index, suggesting that greater change in task engagement is associated with greater PG score change (***Figure 4A***). In support, ΔPG significantly differed across modulation index quartiles for CA1sup neurons (***Figure 4B***). Interestingly, only bottom-quartile neurons exhibited learning-dependent change in PG with a significant reduction after learning, suggesting that the reduction in ACC→CA1 communication is mediated primarily by the loss of connectivity with task-inactive CA1sup neurons (***Figure 4B and C***). Together, these results suggest that CA1sup neurons that are more strongly suppressed during new learning are more likely to become functionally decoupled from the ACC after learning. By contrast, CA1deep exhibited no significant changes across any of these measures further supporting more stable connectivity with ACC (***Figure 4D–F***). Finally, we examined ACC STA of CA1 sublayers. CA1sup showed a significant pre-to-post reduction in baseline-subtracted STA response, whereas CA1deep did not (***Figure 1—figure supplement 1***). However, the direct comparison of pre-to-post change between CA1sup and CA1deep was not significant (p=0.09).

Overall, ACC→CA1sup predictive relationships were less stable across pre- and post-training sleep, with learning-related reductions occurring specifically among task-inactive CA1sup neurons. In contrast, ACC→CA1deep communication remained largely stable across learning. Together, these findings indicate that learning selectively remodels ACC communication with CA1sup neurons, whereas ACC→CA1deep communication is comparatively preserved.

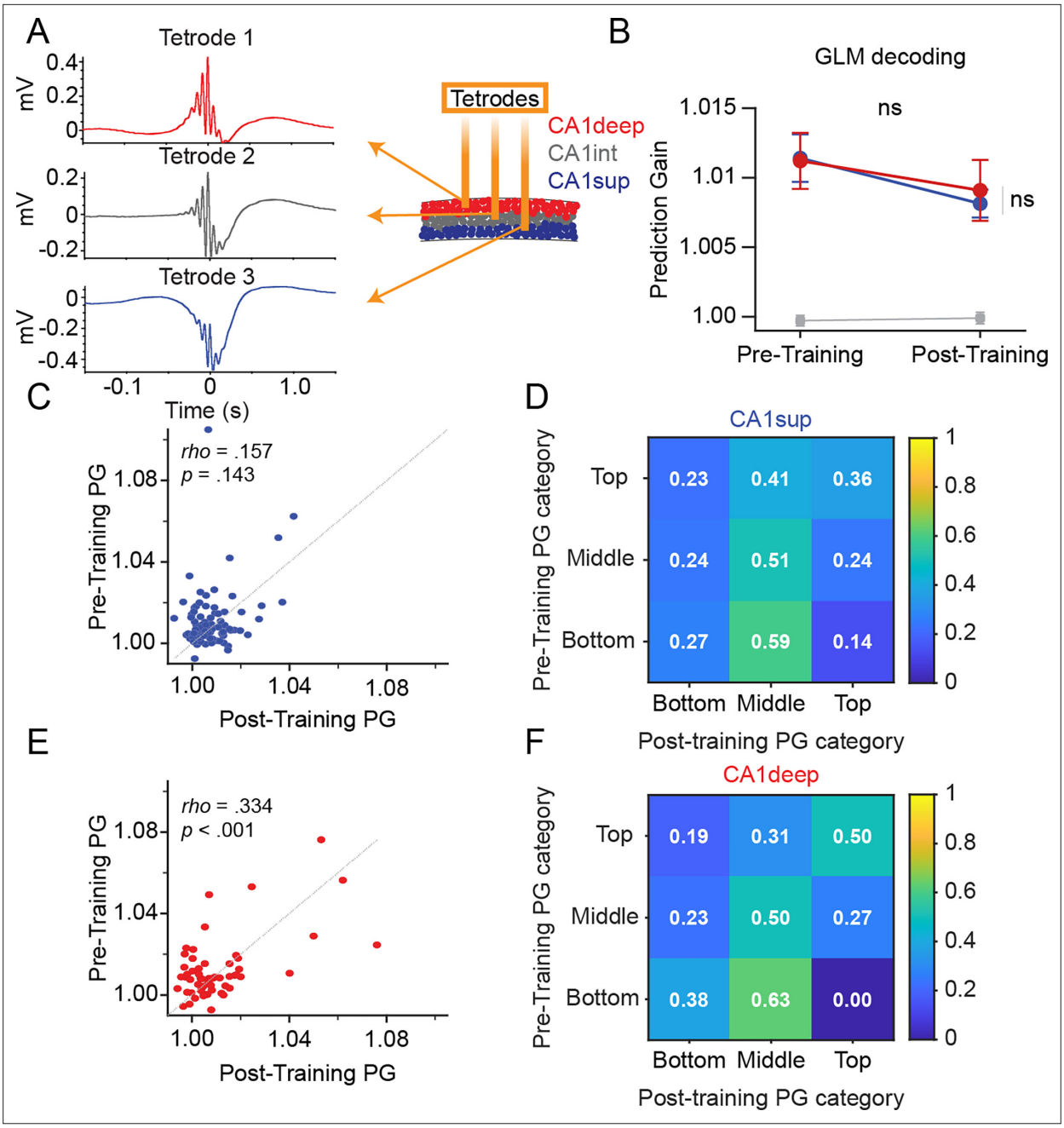


Figure 3. Prediction gain (PG) stability differences between sublayers. (**A**) Schematic of sublayer identification based on sharp-wave deflection difference across the pyramidal layer. (**B**) PG scores before and after learning (N=10 animals; CA1sup: N=89; CA1deep: N=61). Mixed-effects model revealed no significant difference in PG scores between sublayers (p=0.755) but showed a trend for training session (p=0.058). (**C**) Correlation scatter plot of PG score and modulation index for CA1sup neurons (N=89). Spearman's rho revealed no correlation between pre-training and post-training PG scores (rho = 0.157; p=0.143). (**D**) PG score rank preservation permutation matrices for CA1sup neurons (N=89). Permutation testing revealed that neither top-quartile (36.4%, p=0.121) nor bottom-quartile (27.3%, p=0.484) retention exceeded chance levels. (**E**) Correlation scatter plot of PG score and modulation index for CA1deep neurons (N=61). Spearman's rho revealed a significant positive correlation between pre- and post-training PG scores for CA1deep neurons (rho = 0.334; p<0.001). (**F**) PG score rank preservation permutation matrices for CA1deep neurons (N=61). CA1deep neurons' top-quartile retention was 50.0% and significantly above chance, permutation p=0.014. In contrast, bottom-quartile retention did not exceed chance levels, p=0.174. Extreme top-to-bottom or bottom-to-top switching occurred in eight CA1sup neurons (18.2%, p=0.902) and three CA1deep neurons (9.4% p=0.998). Error bars indicate ± SEM.

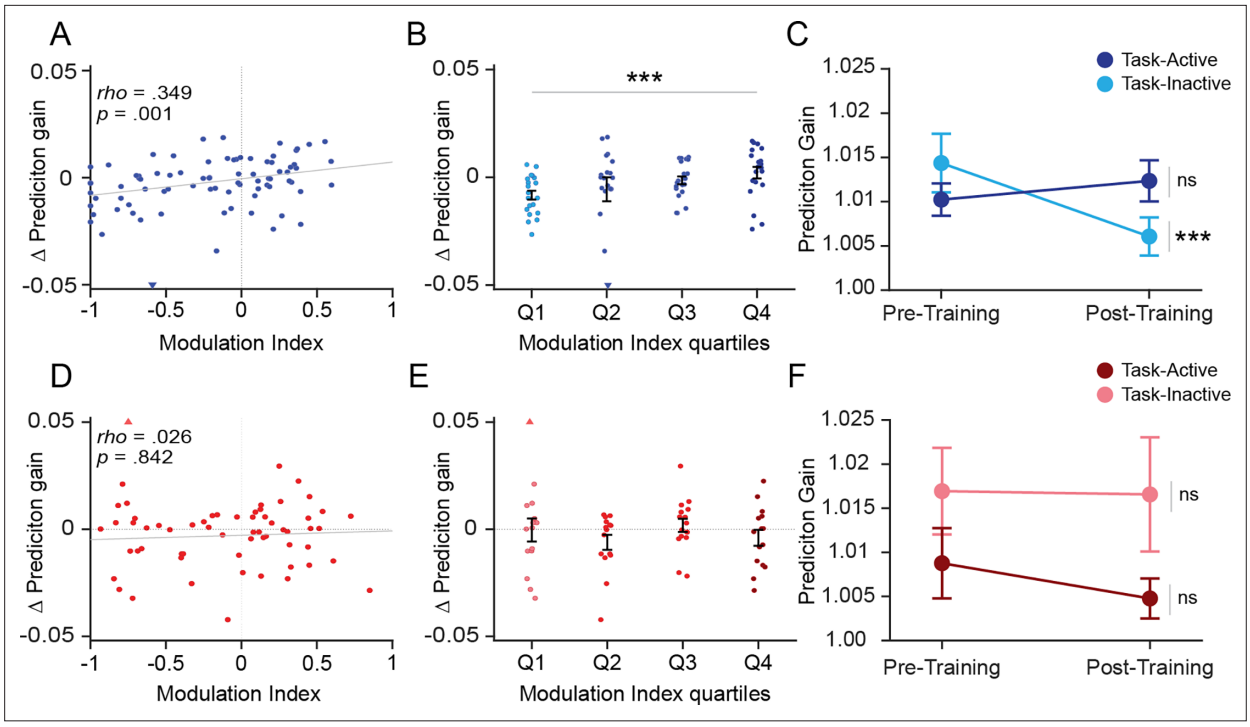


Figure 4. Sublayer differences in ACC→CA1 predictive communication as a function of modulation index. (**A–C**) PG score differences across CA1sup neurons with respect to modulation index (N=7 animals; CA1sup: N=81). (**A**) Correlation between CA1sup neurons' ΔPG and modulation index. Spearman's rho revealed a significant positive correlation, rho = 0.349, p<0.001. (**B**) ΔPG as a function of modulation-index quartiles for CA1sup neurons (N=81). A significant effect of modulation-index quartiles was observed (Kruskal–Wallis, p=0.014). (**C**) PG scores of top and bottom quartiles of CA1sup neurons. A linear mixed-effects model revealed a significant main effect of training session (p<0.001) and quartile x session (p=0.002). Post hoc comparisons revealed a significant pre-to-post decrease in PG score for bottom quartile (Holm-corrected, p=0.002), with no change in top-quartile neurons (Holm-corrected, p=0.442). (**D–F**) PG score differences across CA1deep neurons with respect to modulation index (N=6 animals; N=61 CA1deep neurons). (**D**) Correlation between neurons' PG score and modulation index. Spearman's rho revealed a significant positive correlation between ΔPG and modulation index for CA1sup neurons, rho = 0.026, p=0.842. (**E**) ΔPG as a function of modulation-index quartiles for CA1deep neurons (N=61). CA1deep exhibited no significant effect of modulation-index quartile was observed (Kruskal–Wallis, p=0.591). (**F**) PG scores of top and bottom quartiles of CA1 CA1deep neurons. A linear mixed-effects model did not reveal a significant main effect of training session (p=0.149) or quartile x session interaction (p=0.934). Likewise, post hoc comparisons revealed no changes pre-to-post PG scores for either quartile (bottom quartile: N=15, Holm-corrected, p=0.906; top quartile: N=15, Holm-corrected, p=1). A linear mixed-effects model revealed a trend-level Modulation Index × Sublayer interaction (p=0.063). Error bars indicate ± SEM.

Optogenetic stimulation of the ACC preferentially inhibits CA1sup neurons

To determine whether the ACC can directly influence the activity of CA1sup neurons, we performed optogenetic stimulation of ACC neurons in a separate cohort of mice while recording CA1 neurons during sleep. We microinjected AAV-CaMKII-ChR2 into the ACC and implanted an optic fiber above the injection site, alongside a recording tetrode array implanted into the CA1 ipsilaterally (***Figure 5—figure supplement 1***). After allowing time for viral expression, we administered four-pulse, 25 Hz optogenetic stimulations during sleep to examine how CA1 neurons responded to ACC stimulations. CA1sup neurons displayed prolonged activity changes, primarily suppression, whereas CA1deep showed limited responses (***Figure 5C***). To quantify CA1 sublayer differences, we normalized CA1 firing rates across the stimulation window (0–4 s from stimulation onset) and compared pre-stim to post-stim normalized firing rate (***Figure 5D***). We found that CA1sup firing rate was significantly lower than CA1deep neurons during the 4-s post-stim window. Of note, we replicated these stimulation parameters during wakefulness and found more muted responses across each sublayer, suggesting communication between ACC and CA1 is state-dependent (***Figure 5—figure supplement 2***). Overall, activating ACC produces long-lasting inhibition of CA1sup with limited impact over CA1deep neurons, supporting a selective ACC→CA1sup communication during sleep.

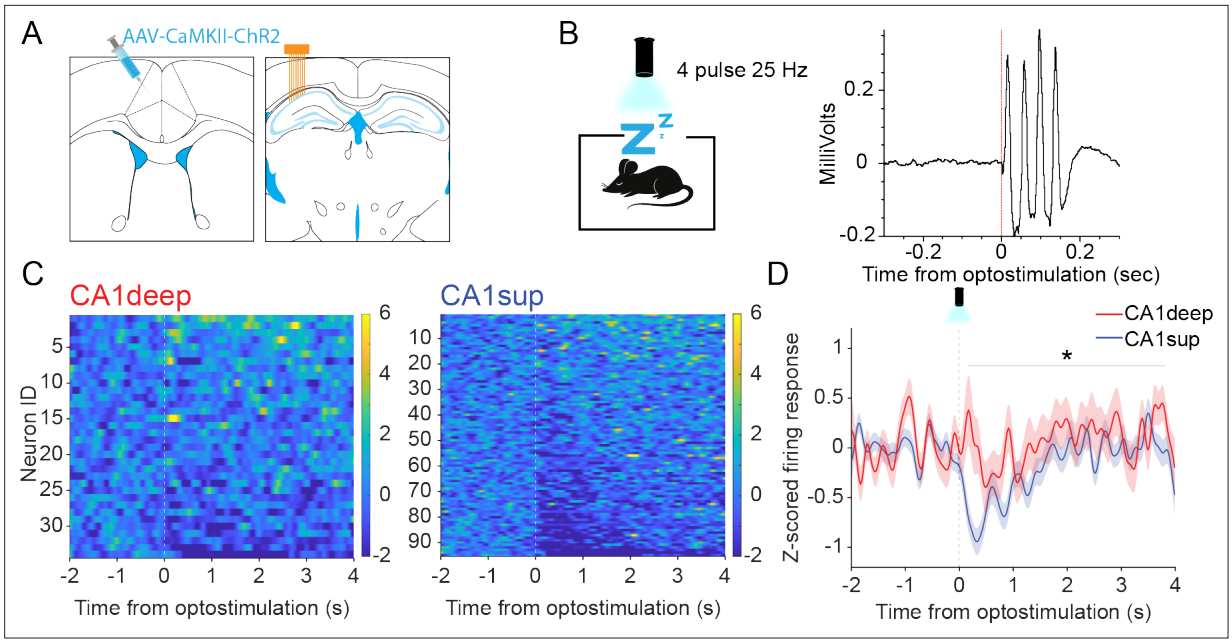


Figure 5. Optogenetic stimulation of the ACC preferentially inhibits CA1sup neurons. (**A**) Schematic of AAV injection and microdive implant. (**B**) Left: schematic of optogenetic manipulation. Four pulse 25 Hz stimulations were performed during home-cage sleep. Right: representative CA1 LFP response to ACC stimulations. A fast peak, indicating maximal inhibition, occurs approximately 13 ms after stimulation onset. (**C**) Heatmap activity CA1deep (N=34) and CA1sup neurons (N=96). (**D**) Linear mixed-effects model revealed a significant Sublayer × Window interaction for the CA1 activity following ACC stimulation, p=0.022. There was also an overall sublayer effect, p=0.037. Post hoc between-sublayer comparisons showed that the strongest difference occurred in the 0–1-s window, with CA1sup neurons showing greater suppression than CA1deep (p<0.01, FDR-corrected, *q*=0.028). Other time windows were not significantly different after FDR correction. Shaded region indicates mean ± SEM.

The online version of this article includes the following figure supplement(s) for figure 5:

Figure supplement 1. Representative histology for optogenetic experiments.

Figure supplement 2. CA1 pyrimdal neuron response to ACC stimulation during wakefulness.

Figure supplement 3. Per-animal CA1 pyramidal neuron responses to ACC stimulation.

Optogenetic stimulation of the ACC differentially affects CA1 interneurons

Within CA1 lies a complex network of interneurons, which play critical roles in memory processes (***Tzilivaki et al., 2023***). We aimed to understand how local interneurons within CA1 respond to ACC stimulations. We first investigated the responses of fast-spiking putative parvalbumin (PV) interneurons. Their firing properties have been well characterized and have been shown to display increased activity during ripples (***Figure 6A–C***; see 'Methods' for details; ***Klausberger and Somogyi, 2008***; ***Opalka et al., 2020***; ***Varga et al., 2014***). Upon stimulation of the ACC during sleep, we discovered a robust inhibition of PV interneurons (***Figure 6D and E***). Like CA1sup neurons, PV suppression was delayed (median latency = 97.5 ms, IQR = 37.5–295 ms) and prolonged, demonstrating that the ACC can drive sustained suppression of both CA1sup and PV interneurons (***Figures 5C and 6E***, ***Figure 6—figure supplement 1E***).

Notably, CA1 LFPs exhibited a laser-evoked response peaking roughly 13 ms after ACC stimulation, which precedes many of the responses seen in PV interneurons and CA1sup neurons (median latency = 350 ms, IQR = 130–830 ms) (***Figures 5B and C and 6E***, ***Figure 6—figure supplement 1E***). This suggests the presence of a different population of CA1 neurons that respond on a scale similar to that seen in the CA1 LFP. Throughout our recording sessions, we noticed a reoccurring neuron type that showed a V-shape spike waveform and distinct autocorrelegram (***Figure 6A and B***). Unlike PV interneurons and pyramidal neurons, these V-type interneurons decreased activity during ripples (***Figure 6C***). Most notable, however, was their robust, low-latency activation to ACC stimulations (median latency = 10.5 ms, IQR = 8.1–13.3 ms) (***Figure 6D***, ***Figure 6—figure supplement 1E***). Overall, these V-type interneurons had a narrow spike width, were fast spiking (Hz), and displayed

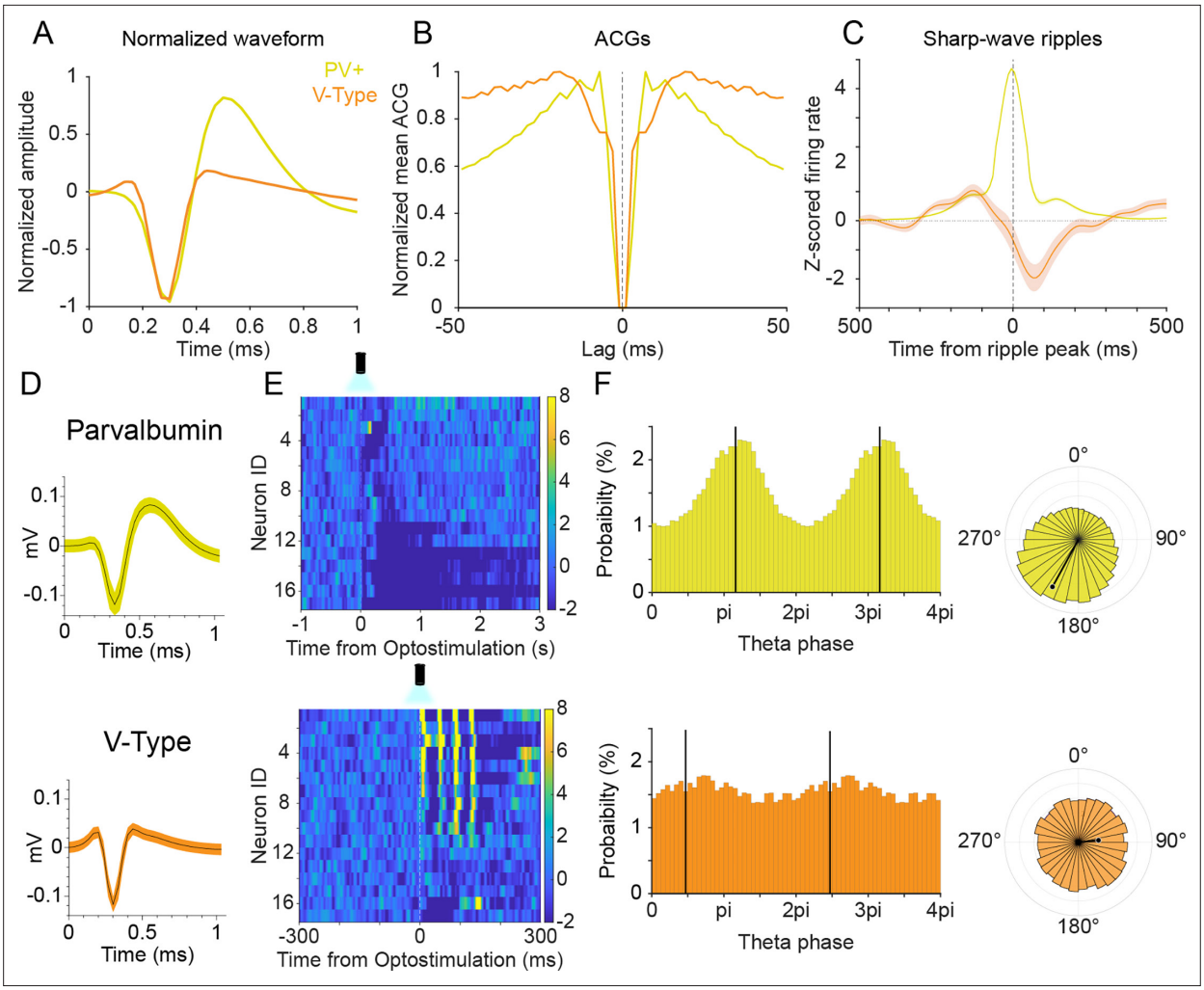


Figure 6. Optogenetic stimulation of the ACC differentially affects CA1 interneurons. (**A**) Normalized waveform of putative PV (N=17) and V-type interneurons (N=17). (**B**) Autocorrelograms (ACGs) of putative PV and V-type interneurons across all spikes. ACGs were calculated for each putative PV and V-type interneuron, then averaged across all neurons within each group. (**C**) Normalized firing across population PV and V-type interneurons during sharp-wave ripples. Mann–Whitney *U* revealed a significant difference in activity during sharp-wave ripples across interneurons, p<0.001. (**D**) Top: representative waveform of putative PV interneuron. Bottom: representative waveform of a V-type interneuron. (**E**) Top: heatmap of PV interneurons spiking activity following stimulation of the ACC (bin size, 5 ms; N=17). Bottom: heatmap of V-type interneurons spiking activity following stimulation of the ACC (bin size, 1 ms; N=17). (**F**) Theta phase-locking analysis and per-neuron circular statistics for CA1 interneurons during active wakefulness theta. Top: PV interneuron phase-locking response during theta. PV interneurons showed significant phase locking at 28.8° relative to trough, *r*=–0.795, Rayleigh p<0.001. Bottom: V-type interneuron phase-locking response during theta. V-type interneurons showed a per-neuron circular mean preferred phase of 84.5° relative to trough; however, this was not significant, *r*=0.385, Rayleigh p=0.079. Per-neuron circular statistics showed that PV and V-type interneurons differed in preferred theta phase (Watson–Williams, p<0.001) and phase-locking strength (Mann–Whitney *U* test, p<0.001). Shaded region indicates mean ± SEM.

The online version of this article includes the following figure supplement(s) for figure 6:

Figure supplement 1. Putative classifications of CA1 neurons.

Figure supplement 2. Per-animal CA1 interneurons response to ACC stimulation.

a distinct inter-spike interval pattern compared to PV interneurons and pyramidal cells (***Figure 6—figure supplement 1***). Unlike PV interneurons, V-type interneurons did not exhibit significant theta phase locking, instead firing more uniformly across the theta cycle, and displayed a significantly lower burst index (***Figure 6F***, ***Figure 6—figure supplement 1D***). Given that V-type interneuron activation precedes suppression of pyramidal cells and PV interneurons after ACC stimulation, it is possible that V-type interneurons mediate the inhibition seen in pyramidal cells and PV interneurons. However, further studies are needed to identify and test whether these neurons influence CA1 network activity.

Discussion

Balancing network excitability with suppression after learning has long been thought to be essential for memory formation, with sleep serving a key homeostatic role (***Liu et al., 2010***; ***Tononi and Cirelli, 2003***; ***Tononi and Cirelli, 2006***; ***Watson et al., 2016***). Excessive excitability and overly strengthened synapses can hinder neuronal flexibility and saturate the capacity for learning (***Balduzzi and Tononi, 2013***; ***Gava et al., 2024***; ***Norimoto et al., 2018***). Additionally, underregulated excitability may pathologically link multiple memory traces, leading to memory overgeneralization (***Jinde et al., 2012***; ***Kim et al., 2021***). Therefore, regulatory mechanisms that rebalance the excitability of neurons to enable neuronal flexibility are essential for memory formation (***Gava et al., 2024***; ***Karaba et al., 2024***). CA1sup neurons have been shown to be particularly susceptible to memory rigidity (***Gava et al., 2024***; ***Hall and Wang, 2023***). While activation of these neurons is necessary for the encoding of new memories, their regulation and timely suppression appear equally important to evoke flexibility and enable de novo consolidation within the hippocampal network (***Gava et al., 2024***; ***Harvey et al., 2023***). Our results reveal a rebalancing of communication between the ACC and CA1 following learning. This was most pronounced for CA1sup neurons as functional connectivity was dynamically reorganized between pre- and post-training sleep. In particular, pre-existing ACC-to-CA1sup communication was weakened for task-inactive neurons after learning. Furthermore, we found that optogenetic ACC stimulations preferentially inhibited CA1sup neurons. Overall, our study uncovers an ACC→CA1sup line of communication that adapts to learning, potentially playing a role in the rebalancing of network excitability for memory formation.

Learning selectively weakens ACC coupling with task-inactive CA1sup neurons

We implemented GLM machine learning to decode CA1 neuronal firing rates during ripples based on the spiking rates of large ACC neuronal populations preceding ripples (***Rothschild et al., 2017***). The underlying principles of this analysis posit that if ACC activity preceding ripples influences subsequent activity in CA1 during ripples, the specific activity pattern of ACC neurons (predictor cells) should hold relevancy over the outcome of CA1 neurons (predicted cells). We found this to be true across all sleep sessions and neuron types, with real ACC spiking data showing significantly higher prediction gain compared to shuffled data, indicating an information flow from ACC to CA1 surrounding ripples. Interestingly, prediction gain was weakened following learning specifically for task-inactive CA1sup neurons, suggesting a selective reorganization of communication with CA1sup neurons according to their recruitment during training. However, questions remain over exactly how the ACC influences CA1sup activity and why this information flow rebalances after learning.

One possible explanation is that ACC→CA1sup communication before training may reflect encoding of past experiences. Research has demonstrated that the ACC has a limited role in consolidation immediately after learning (***Liu et al., 2024a***). Instead, memories become ACC-dependent beginning typically 2 days after learning (***Einarsson and Nader, 2012***; ***Frankland et al., 2004***; ***Liu et al., 2024a***). It is possible that heightened pre-existing communication between ACC and CA1sup is reflective of consolidating past experiences. If true, decreased communication between regions may be due to the network's shift toward prioritizing the encoding/consolidating of the new experience and thus the role of the ACC to CA1, consolidating past memories, is reduced (***Diekelmann and Born, 2010***; ***Huelin Gorriz et al., 2023***; ***Wilson and McNaughton, 1994***). From a broader perspective, ACC→CA1 could function as part of default mode network activity, and learning induces network shift toward the newly acquired memory (***Buckner et al., 2008***; ***Raichle, 2015***).

Alternatively, ACC→CA1 communication may contribute to the homeostatic downscaling of memory-unrelated synapses during sleep. Evidence finds that slow-wave sleep is strongly linked to downscaling of non-learning-related neuron activity (***Gulati et al., 2017***; ***Liu et al., 2010***; ***Tononi and Cirelli, 2003***; ***Tononi and Cirelli, 2006***; ***Watson et al., 2016***). Slow-wave sleep ripples in particular depotentiate memory-unrelated synapses (***Gulati et al., 2017***; ***Norimoto et al., 2018***). In our study, we find that the learning-related reduction in communication between ACC and CA1 was selective for task-inactive neurons. Therefore, ACC→CA1sup communication may not simply weaken following learning but rather becomes selectively disengaged from task-inactive neurons, enabling homeostatic downscaling while preserving behaviorally relevant synapses (***Liu et al., 2010***; ***Norimoto et al., 2018***; ***Tononi and Cirelli, 2003***; ***Tononi and Cirelli, 2006***; ***Watson et al., 2016***). Interestingly,

behavioral recruitment alone cannot account for the observed remodeling of ACC→CA1 communication, as CA1sup and CA1deep neurons did not display significant differences in task-related activity (***Figure 2—figure supplement 2***). Instead, these learning-related changes of task-inactive neurons appear sublayer specific.

A potential mechanism supporting this selectivity is suggested by our optogenetic findings, which revealed preferential suppression of CA1sup neurons following ACC stimulations. ACC-mediated inhibition may contribute to the gradual disengagement of subsets of CA1sup neurons over time as memories transition toward long-term storage (***Karaba et al., 2024***; ***Raven and Aton, 2021***). Such a mechanism would align with ACC's known role in systems consolidation and be particularly useful in the regulation of CA1sup neurons as they have been shown to be susceptible to memory rigidity and overgeneralization (***Einarsson and Nader, 2012***; ***Frankland et al., 2004***; ***Gava et al., 2024***; ***Liu et al., 2024a***). Future experiments casually manipulating this communication are needed to determine whether ACC activity directly influences the downregulation of CA1sup activity during training, or whether these regions are correlated partners whose activity is ultimately mediated by an external brain region.

As research investigating CA1 heterogeneity continues to gain attention, functional distinctions across different behaviors have emerged (***Hall and Wang, 2023***). Previous research has found that CA1deep neurons are more involved in reward and sensory landmark encoding, while CA1sup neurons are more involved in context and spatial encoding (***Danielson et al., 2016***; ***Geiller et al., 2017***; ***Harvey et al., 2023***). Moreover, CA1deep place cells are more likely to remap in response to local cue changes than CA1sup place cells (***Esparza et al., 2025***). There have been conflicting reports over which sublayer is more involved in learning and replay and which neurons are more plastic or rigid in response to learning (***Berndt et al., 2023***; ***Geiller et al., 2017***; ***Grosmark and Buzsáki, 2016***; ***Hall and Wang, 2023***; ***Harvey et al., 2023***). We speculate that it may depend on the behavioral task and the relevant upstream circuits that differentially recruit CA1 sublayers (***Masurkar et al., 2017***). Past reports, which have shown that CA1sup neurons are more involved in memory replay, implemented spatial learning tasks (***Berndt et al., 2023***; ***Harvey et al., 2023***). In contrast, CA1deep neurons have been shown to be more important for encoding non-spatial aspects of memories, such as reward (***Danielson et al., 2016***; ***Harvey et al., 2023***). In our study, we did not observe clear differences in sublayer responses to CFC. Instead, we uncovered a pathway-specific difference with ACC→CA1sup displaying a more plastic-like phenotype in response to learning compared to ACC→CA1deep. These findings, along with past reports, suggest that functional differences between CA1 sublayers may be better understood in the context of the specific behavioral and upstream circuits engaged during learning rather than as fixed 'plastic' or 'rigid' properties of the sublayers themselves (***Masurkar et al., 2017***). In fact, recent findings further complicate this notion, demonstrating sublayer differences emerging between two classes of ripples that differ based on current source density profiles (***Castelli et al., 2025***). Ultimately, future studies are needed to fully dissect the functional differences among CA1 sublayers and their inputs during ripples and across behaviors.

Lastly, our CA1 sublayer classification does come with its own caveats. Tetrode identification of CA1 sublayers is not a trivial matter. We implemented guidelines informed by past research (see 'Methods') to help ensure we isolated CA1sup and CA1deep groups, only including neurons where we had the greatest confidence (***Berndt et al., 2023***; ***Mizuseki et al., 2011***). In doing so, we excluded neurons whose classification was uncertain. It is possible this excludes some meaningful populations of CA1 sublayers. Additionally, despite our approach, some cross-inclusion of sublayers may remain. Therefore, interpretations of CA1 sublayers' difference should be considered with these limitations in mind. That said, the number of neurons and animals tested does provide overall confidence regarding our results. Future studies investigating this ACC to CA1 sublayer-specific line of communication would benefit from the use of silicon probes or neuropixels that enable precise radial localization. Another caveat to mention is that both the ACC and CA1 are involved in the stress response (***Kim et al., 2015***; ***Lamotte et al., 2021***). Future experiments utilizing appetitive learning paradigms, rather than the aversive CFC used here, will help disentangle learning-related remodeling of ACC→CA1 communication from changes driven by stress.

Optogenetic stimulation of the ACC inhibits CA1sup neurons and PV interneurons

We found that direct stimulation of ACC excitatory neurons inhibited CA1sup and PV interneurons. Notably, these responses were delayed for CA1sup and PV interneurons, indicating polysynaptic connectivity (***Piñol et al., 2012***). Additionally, both neuron types exhibited sustained suppression in response to stimulations suggesting that the ACC may have an indirect and broad influence over CA1 network activity rather than a direct and transient role. Sustained inhibition over certain populations of pyramidal neurons and PV interneurons may support a rebalancing of network excitability, especially during sleep (***Diekelmann and Born, 2010***; ***Norimoto et al., 2018***; ***Tononi and Cirelli, 2003***).

The identification of V-type neurons may help explain responses seen in CA1sup and PV interneurons. These neurons displayed the lowest latency responses to stimulations and produced brief excitatory bursts indicative of an initial response to ACC stimulations (***Piñol et al., 2012***). These interneurons decreased their activity during ripples, a pattern that overlaps with *Sncg*-expressing CCK basket cells and inhibitor of DNA binding 2 (ID2) neurons (***Dudok et al., 2021***; ***Karaba et al., 2024***; ***Valero et al., 2025***; ***Vancura et al., 2023***). It is possible that V-type neurons may overlap with these interneurons. Correspondence with CCK cell activity is of particular interest, given the role of CCK interneurons in CA1 circuitry. Namely, CCK interneurons are known to target CA1sup and PV interneurons and induce long-term excitability changes as seen in our optogenetic experiments (***Hefft and Jonas, 2005***; ***Karson et al., 2009***; ***Klausberger et al., 2005***; ***Valero et al., 2015***). More recently, CCK interneurons have been identified as playing a causal role in regulating the excitability of CA1 neurons during ripples (***Karaba et al., 2024***). Together, this suggests a possible ACC influence on CA1 CCK interneurons, which provides sustained inhibition of CA1 pyramidal and PV interneurons during sleep in facilitating memory formation. One discrepancy, however, is that both CCK and ID2 neurons exhibit theta phase preference, which we found no evidence for in V-type interneuron (***Klausberger et al., 2005***; ***Valero et al., 2025***). Ultimately, our interpretations of V-type identity remain speculative as further studies are needed to characterize their activity, and causal experiments are required to completely elucidate their role.

Another important caveat to mention is that it remains an ongoing debate whether ACC directly projects to CA1 (***Andrianova et al., 2023***; ***Rajasethupathy et al., 2015***; ***Shi et al., 2022***). One lab reported monosynaptic ACC to CA1 connection (***Rajasethupathy et al., 2015***), while another lab replicated those same experiments but was unable to come to the same conclusions (***Andrianova et al., 2023***). Further studies report no direct connection (***Shi et al., 2022***). The contention in connectivity may arise from differences in targeting strategies, injection coordinates, or viruses used. Our findings reported an excitatory response in CA1 V-type interneurons in response to ACC stimulations, proposing another possibility for ACC→CA1 connectivity. Interestingly, V-type interneurons responded with low-latency as fast as 4.2 ms after stimulations, compatible with monosynaptic timing (***Cho et al., 2013***; ***Petreanu et al., 2007***; ***Wang et al., 2009***). If the ACC→V-type connection was a monosynaptic pathway, it could help explain discrepancies in the field, as the relative sparsity of V-type interneurons may reduce the likelihood of detecting ACC→CA1 connectivity. However, future anatomical studies are needed to conclusively determine connectivity.

Alternatively, ACC→CA1 communication may be mediated by multiple intermediate structures (***Behzadi et al., 1990***; ***Oh et al., 2014***; ***Shi et al., 2022***; ***Souza et al., 2022***). The ACC sends monosynaptic projections to the nucleus reuniens (RE) and median raphe (MnR), both of which project directly to CA1 (***Oh et al., 2014***; ***Shi et al., 2022***). The RE has a known role in contextual discrimination learning and memory specificity (***Ramanathan and Maren, 2019***; ***Ramanathan et al., 2018***; ***Ratigan et al., 2023***; ***Silva et al., 2021***; ***Xu and Südhof, 2013***). Interestingly, RE→CA1 activity tuned to immobility (freezing) emerges only after shocks are presented, suggesting a learning-induced modification between regions, similar to that seen in our ACC–CA1 data (***Ratigan et al., 2023***). As for MnR, it receives dense inputs from the ACC (***Behzadi et al., 1990***; ***Souza et al., 2022***), and its projections to the CA1 are predominantly glutamatergic (***Jackson et al., 2009***; ***Senft et al., 2021***; ***Szőnyi et al., 2016***). Notably, these glutamatergic MnR inputs directly target CA1 interneurons, including CCK basket cells (***Miettinen and Freund, 1992***; ***Morales and Bloom, 1997***; ***Senft et al., 2021***), while avoiding PV interneurons and pyramidal neurons (***Acsády et al., 1993***; ***Freund et al., 1990***; ***Halasy et al., 1992***; ***Miettinen and Freund, 1992***; ***Papp et al., 1999***; ***Turi et al., 2019***). This connectivity suggests that the ACC may indirectly modulate CA1 activity through the MnR, potentially suppressing

PV interneuron and pyramidal neuron activity via local inhibitory circuits, thereby contributing to the regulation of hippocampal oscillations and memory consolidation (***Huang et al., 2022***; ***Wang et al., 2015***). Ultimately, future experiments combining pathway-specific manipulations with simultaneous recordings will be necessary to distinguish direct from polysynaptic mechanisms.

Methods

Mice

Male C57BL/6 mice were purchased from the Jackson Laboratory (stock #000664). Mice were 3–4 months old at the time of surgery; after surgery, they were singly housed in cages (40 × 20 × 25 cm) containing corn cob and cotton material and kept on a 12 h light/dark cycle with ad libitum access to food and water. Experimental procedures were approved by the Institutional Animal Care and Use Committees of Drexel University (protocol # LA-23-740) and were in accordance with the National Research Council *Guide for the Care and Use of Laboratory Animals*.

Stereotaxic surgery

Surgery procedures were similar to that used in our lab (***Huang et al., 2026***; ***Liu et al., 2024b***; ***Liu et al., 2021***). In brief, mice were anesthetized with a ketamine/xylazine mixture (~100/10 mg/kg, i.p.) and kept on a heating pad at 37°C. For in vivo electrophysiology recording, mice received implantation of two electrode arrays (eight tetrodes each) into the ACC and CA1, respectively (***Lin et al., 2006***). For optogenetic stimulation, mice received intra-ACC microinjection of AAV viruses (AAV1-CKIIa-ChR2-GFP; 0.250 µl; ~10^{13} GC/ml; *Addgene* 105669) and implantation of one optic fiber (diameter 200 µm) slightly above the injection site; meanwhile, they received implantation of eight tetrodes into the CA1 unilaterally on the ipsilateral side. AAV vectors were microinjected through a syringe pump (World Precision Instruments) over 5 min (50 nl/min), with an additional 5 min waiting period before removal of the injection needle (34 gauge, beveled). ACC coordinates from Bregma were AP 0.9 mm, ML 0.3 mm, DV 1.0 mm; CA1 coordinates from Bregma were AP –2.1 mm, ML 1.7 mm, and DV 1.1 mm.

In vivo electrophysiology

Each tetrode consisted of four wires (90% platinum, 10% iridium; 18 µm diameter; California Fine Wire). A microdrive was used to couple with the electrode array, similar to that used in our lab (***Liu et al., 2024b***; ***Liu et al., 2021***; ***Wang et al., 2015***). Neural signal was preamplified, digitized, and recorded using a *Blackrock Neurotech* CerePlex. The LFPs were digitized at 2 kHz and filtered at 500 Hz low cut; spikes were digitized at 30 kHz and filtered between 600 and 6000 Hz. The tetrode arrays were gradually lowered daily until we recorded clear ripples and a substantial number of neurons; otherwise, mice were excluded from the study. The recorded spikes were sorted manually using *Plexon* Offline Sorter. For dual-site experiments, spikes from 10 mice were used for analyses in this study; the neuron numbers in ACC and CA1 were 48/27, 35/50, 28/12, 32/27*, 22/29, 26/17, 28/33, 19/17, 27/47, and 38/32, respectively. For optogenetic and in vivo electrophysiology experiments, five mice were used. The neuron numbers in CA1 were 35, 30, 10, 38, and 24.

* This animal is missing the recording file during training and therefore was excluded from analyses comparing task active/inactive and firing rate ratios during training.

Optogenetics manipulations

Following surgery, mice were given 1 week for recovery and viral expression development. During recording, mice received four-pulse 25 Hz stimulations (20-s inter-trial interval). Laser stimulations ranged between 5–8 mW (473 nm wavelength). Laser intensity was tuned for each recording session until stimulation evoked a >0.2 mV change in CA1 LFP.

Ripples

LFPs were band-pass filtered between 100–250 Hz and ripple envelope was smoothed with a Gaussian kernel (SD=4 ms) (***Karlsson and Frank, 2009***). We defined ripple amplitudes as the peak values of ripple envelopes. Only ripples with amplitudes exceeding 5 SD above the mean were used for analyses. For each ripple, onset and offset were taken as the earliest and latest time points where the

ripple amplitude exceeded 1 SD above the mean around the ripple peak. Ripple duration was the difference between ripple onset and offset. Ripples less than 20 ms were excluded from the analysis.

Modulation and burst index

Modulation index was a firing rate ratio calculated by comparing spiking during training with pre-training sleep baseline (***Girardeau et al., 2017***; ***Karaba et al., 2024***; ***Oliva et al., 2020***). Equation: Modulation index = (Train – Pretrain) / (Train +Pretrain), in which Train and Pretrain are the average spikes per second for each CA1 neuron calculated during training and pre-training sleep, respectively. Burst index was defined as the fraction of consecutive inter-spike intervals shorter than 6ms across the full session recording (***Harris et al., 2001***).

GLM decoding

We constructed GLMs with a log link function to predict spike counts of individual CA1 neurons during ripples based on population spike counts in ACC across specific time windows (***Liu et al., 2024b***; ***Rothschild et al., 2017***). Spike counts of each ACC neuron were binned in 200 ms bins relative to ripple onset: −600 to −400 ms, −400 to −200 ms, −200 to 0 ms to predict CA1 activity 0–100 ms. We randomly partitioned the ripples into two approximately equally sized datasets: one of them was used to train the GLM decoder, and the other was used for testing. The model derived from the training phase was applied to the ACC population spike data in the test set, yielding predictions for the predicted CA1 spike counts across ripples. We calculated a prediction error for each CA1 neuron that was the mean absolute error between the predicted spike rate and real spike rate. We replicated this same analysis for shuffled data; wherein shuffled error distribution was generated by randomly permuting the predicted CA1 spike counts across ripple events. Prediction gain scores were derived by dividing shuffled prediction error by the real prediction error. Slow-wave sleep was determined by animals' immobility and the theta (6–12 Hz) /delta (1–4 Hz) ratio extracted from the local field potentials. A ratio of 1 or lower was identified as SWS; only epochs greater than 10 min were selected (***Wang et al., 2015***).

ACC activity surrounding ripples

To calculate significant differences in ACC activity surrounding ripples, we computed peri-ripple event histograms (smoothed with a three-bin Gaussian filter; bin size, 5 ms) for individual ACC neurons. We then compared ACC spiking activity between two 250 ms windows starting either –200 ms or –2000 ms (baseline) before ripple onset. 235 neurons (94%) showed significant increase from baseline (Wilcoxon signed-rank $p<0.01$). Pre- or post-ripple peaks were determined whether a neuron's firing rate peaked before (–200 to 0 ms) or after (0–200 ms) ripple onset.

Classification of CA1 pyramidal and interneurons

Putative excitatory (pyramidal) neurons and parvalbumin fast-spiking interneurons were classified based on spike waveform, firing rate, and spike width (***Opalka et al., 2020***; ***Figure 6—figure supplement 1A–C***). V-type interneurons were classified based on waveform, firing rate, spike width, and decreased ripple-correlated activity (***Figure 6—figure supplement 1A–C***). For sublayer classification, we examined the mean amplitude of the sharp-wave deflection at maximum ripple power for each tetrode. Sharp-wave deflections that were greater than 50 μV were classified as CA1deep sublayer, whereas deflections less than –50 μV were classified as CA1sup sublayer. Any deflections between –50 and 50 μV were treated as intermediate and were excluded from sublayer analyses (***Figure 3A***).

Response latency to ACC optogenetic stimulations

Neural activity following stimulation onset was binned (CA1sup, 20 ms; PV, 5 ms; V-type, 0.1 ms) and z scored. For PV interneurons and CA1sup neurons, response latency was obtained by selecting the first bin where a neuron showed a difference from the baseline by a z-score of ±2 or more (minimum for three consecutive bins). Because V-type interneurons exhibited substantially shorter response latencies, a higher temporal resolution analysis was performed. Spikes were aligned to four-pulse optogenetic stimulation trains and binned at 0.1 ms resolution. Firing rates during inter-pulse windows were z-scored relative to baseline, and response latency was defined as the time from stimulation onset to

the peak response in the window with the strongest activation. Only neurons with a maximal response of z≥5 were included in the latency analysis.

Spike-theta phase locking

Theta oscillations were obtained from CA1 LFPs filtered at 6–12 Hz using a zero-phase filter in MATLAB (bandpass IIR filter; filter order = 8). Theta phase was estimated by Hilbert transformation of the filtered signal. For each neuron, spike times occurring during selected theta epochs were matched to the nearest LFP sample, and the corresponding instantaneous theta phase was extracted for circular statistical analysis. Phase locking was quantified using CircStat functions (***Berens, 2009***). We used the standard Rayleigh test to determine the uniformity of phase distribution (***Totah et al., 2013***), in which the p value for circular uniformity is calculated as follows:

$$p = exp(sqrt(1 + 4^*n + 4^*(n^2 - R^2)) - (1 + 2^*n))$$

and Rayleigh's *z* to determine the strength of spike–LFP phase locking as follows:

$$z = R^2/n$$

where *R* is the sum of resultant vectors across *n* spikes. Log-transformed Rayleigh *z* values were calculated log *z* values and stored for each neuron/group.

Spike-triggered average (STA)

For each CA1 neuron, all ACC spikes recorded during slow-wave sleep in that same session were pooled and used as reference events. The spike times of each CA1 neuron were aligned to the pooled ACC spike. Relative CA1 spike times were counted in 10 ms bins over a window spanning −200 to 300 ms relative to the pool ACC spike. Spike counts within each lag bin were summed across all ACC spikes and converted to firing rate (Hz) by dividing by the total number of ACC spikes and the bin width. To normalize each neuron's lag-resolved STA, the mean firing rate during the −200 to −100 ms pre-ACC-spike baseline window was subtracted from every lag bin for that neuron. Thus, the normalized STA curve estimates the change in CA1 firing rate relative to the pre-ACC-spike baseline as a function of time from ACC spiking. Full-lag significance was assessed using an animal-level sign-flip cluster permutation test (***Maris and Oostenveld, 2007***). Post-minus-Pre STA difference curves were calculated for each animal, contiguous lag bins exceeding an uncorrected paired-test threshold were grouped into clusters and observed cluster masses were compared against a 5000-permutation sign-flip null distribution.

Fear conditioning (in vivo recording)

The fear-conditioning chamber used in the experiment was a square chamber measuring 25 × 25 × 32 cm, with a 36 bar shock grid floor (Med Associates). The behaviors of the mice were recorded using Blackrock Neurotech NeuroMotive video system. During training, the mice were first allowed to explore the footshock chamber for 3 min. They then received three mild footshocks (0.75 mA, 0.5 s), with a 2 min interval between shocks. About 30 s after the last shock, the mice were returned to their home cages. After ~2 h of post-training sleep, the mice were placed back in the footshock chamber for a 5 min contextual fear test. Neural activity was recorded continuously, including the pre-training sleep (2–3 h), training (7.5 min), post-training sleep (2–3 h), and contextual-fear test (5 min). Freezing was defined as the absence of visible movement except for respiration as previously described and was scored continuously during the recall test (***Anagnostaras et al., 2003***; ***DeLorey et al., 1998***). Percent Freezing was defined as time spent freezing divided by total time in recall (or pre-shock baseline during CFC). Additionally, the day prior to fear conditioning, mice were placed into a novel box for 7.5 min; neural activity was recorded across the pre-exposure sleep, exposure, and post-exposure sleep phases, to act as a behavioral control; however, these datasets were not analyzed for this manuscript.

Histology

To mark the final recording sites, we made electrical lesions by passing 20 s, 10-μA currents through two or more tetrodes. Mice were deeply anesthetized and intracardially perfused with ice-cold PBS or

saline, followed by 10% formalin. The brains were removed and postfixed in formalin for at least 24 h. The brains were sliced into coronal sections of 50 μm thickness using Leica vibratome. Sections were mounted with Mowiol mounting medium mixed with DAPI for microscopic examination of electrode placements, viral vector expression, and/or optical fiber placements.

Statistics

Sample sizes were based on previous similar studies in our labs (***Liu et al., 2024b***; ***Liu et al., 2021***; ***Wang et al., 2015***). Other statistical analyses include Friedman's test, Wilcoxon signed-rank test, Mann–Whitney *U* test, Kruskal–Wallis test, Welch's *t*-test, independent-sample *t*-test, and Student's *t*-test. All statistical tests were two-sided. p-values of 0.05 or lower were considered significant. Non-parametric tests were utilized when normality assumptions failed.

Acknowledgements

We thank the members of the Drexel ULAR staff for support and Dr. Wen-Jun Gao, Shayna Singh, Ashley Opalka, and Wenqiang Huang for their thoughtful comments. This work was supported by NIH F31 MH134582 (AFH) and R01MH119102 (DVW).

Additional information

Competing interests

Dong V Wang: Reviewing editor, eLife. The other author declares that no competing interests exist.

Funding

Funder	Grant reference number	Author
National Institute of Mental Health	R01MH119102	Dong V Wang
National Institute of Mental Health	F31 MH134582	Arron F Hall

The funders had no role in study design, data collection and interpretation, or the decision to submit the work for publication.

Author contributions

Arron F Hall, Dong V Wang, Conceptualization

Author ORCIDs

Arron F Hall https://orcid.org/0000-0002-7680-406X
Dong V Wang https://orcid.org/0000-0001-8537-5677

Ethics

All experimental procedures were approved by the Institutional Animal Care and Use Committees at Drexel University (Protocol # LA-23-740) and adhered to the National Research Council's Guide for the Care and Use of Laboratory Animals.

Peer review material

Version of Record:
Reviewer #2 (Public review): https://doi.org/10.7554/eLife.107370.3.sa1
Author response https://doi.org/10.7554/eLife.107370.3.sa2

Reviewed preprint v2
Reviewer #2 (Public review): https://doi.org/10.7554/eLife.107370.2.sa1
Author response: https://doi.org/10.7554/eLife.107370.2.sa0
eLife Assessment https://doi.org/10.7554/eLife.107370.2.sa2

Reviewed preprint v1

Reviewer #1 (Public review): https://doi.org/10.7554/eLife.107370.1.sa3
Reviewer #2 (Public review): https://doi.org/10.7554/eLife.107370.1.sa2
Reviewer #3 (Public review): https://doi.org/10.7554/eLife.107370.1.sa1
Author response: https://doi.org/10.7554/eLife.107370.1.sa0
eLife Assessment https://doi.org/10.7554/eLife.107370.1.sa4

Additional files

Supplementary files

MDAR checklist

Data availability

Data and code are publicly available at: https://doi.org/10.6084/m9.figshare.33467404. Key MATLAB scripts used in this study have been deposited to a public repository (https://github.com/DVWangLab/Hall-and-Wang-eLife-2026; copy archived at ***Wang, 2026***).

The following dataset was generated:

Author(s)	Year	Dataset title	Dataset URL	Database and Identifier
Hall AF, Wang DV	2026	A cortical-hippocampal communication undergoes rebalancing after new learning	https://doi.org/10.6084/m9.figshare.33467404	figshare, 10.6084/m9.figshare.33467404

References

Acsády L, Halasy K, Freund TF. 1993. Calretinin is present in non-pyramidal cells of the rat hippocampus--III. Their inputs from the median raphe and medial septal nuclei. *Neuroscience* **52**:829–841. DOI: https://doi.org/10.1016/0306-4522(93)90532-k, PMID: 7680801

Anagnostaras SG, Murphy GG, Hamilton SE, Mitchell SL, Rahnama NP, Nathanson NM, Silva AJ. 2003. Selective cognitive dysfunction in acetylcholine M1 muscarinic receptor mutant mice. *Nature Neuroscience* **6**:51–58. DOI: https://doi.org/10.1038/nn992, PMID: 12483218

Andrianova L, Yanakieva S, Margetts-Smith G, Kohli S, Brady ES, Aggleton JP, Craig MT. 2023. No evidence from complementary data sources of a direct glutamatergic projection from the mouse anterior cingulate area to the hippocampal formation. *eLife* **12**:e77364. DOI: https://doi.org/10.7554/eLife.77364, PMID: 37545394

Balduzzi D, Tononi G. 2013. What can neurons do for their brain? Communicate selectivity with bursts. *Theory in Biosciences = Theorie in Den Biowissenschaften* **132**:27–39. DOI: https://doi.org/10.1007/s12064-012-0165-0, PMID: 22956291

Behzadi G, Kalén P, Parvopassu F, Wiklund L. 1990. Afferents to the median raphe nucleus of the rat: retrograde cholera toxin and wheat germ conjugated horseradish peroxidase tracing, and selective D-[3H]aspartate labelling of possible excitatory amino acid inputs. *Neuroscience* **37**:77–100. DOI: https://doi.org/10.1016/0306-4522(90)90194-9, PMID: 2243599

Berens P. 2009. CircStat: a MATLAB toolbox for circular statistics. *Journal of Statistical Software* **31**:1–21. DOI: https://doi.org/10.18637/jss.v031.i10

Berndt M, Trusel M, Roberts TF, Pfeiffer BE, Volk LJ. 2023. Bidirectional synaptic changes in deep and superficial hippocampal neurons following in vivo activity. *Neuron* **111**:2984–2994. DOI: https://doi.org/10.1016/j.neuron.2023.08.014, PMID: 37689058

Buckner RL, Andrews-Hanna JR, Schacter DL. 2008. The brain's default network: anatomy, function, and relevance to disease. *Annals of the New York Academy of Sciences* **1124**:1–38. DOI: https://doi.org/10.1196/annals.1440.011, PMID: 18400922

Buzsáki G, Horváth Z, Urioste R, Hetke J, Wise K. 1992. High-frequency network oscillation in the hippocampus. *Science* **256**:1025–1027. DOI: https://doi.org/10.1126/science.1589772, PMID: 1589772

Buzsáki G. 2015. Hippocampal sharp wave-ripple: A cognitive biomarker for episodic memory and planning. *Hippocampus* **25**:1073–1188. DOI: https://doi.org/10.1002/hipo.22488, PMID: 26135716

Castelli M, Lopes-dos-Santos V, Gava GP, Lambiotte R, Dupret D. 2025. Hippocampal ripple diversity organises neuronal reactivation dynamics in the offline brain. *bioRxiv*. DOI: https://doi.org/10.1101/2025.03.11.642571

Cho JH, Deisseroth K, Bolshakov VY. 2013. Synaptic encoding of fear extinction in mPFC-amygdala circuits. *Neuron* **80**:1491–1507. DOI: https://doi.org/10.1016/j.neuron.2013.09.025, PMID: 24290204

Danielson NB, Zaremba JD, Kaifosh P, Bowler J, Ladow M, Losonczy A. 2016. Sublayer-specific coding dynamics during spatial navigation and learning in hippocampal area CA1. *Neuron* **91**:652–665. DOI: https://doi.org/10.1016/j.neuron.2016.06.020, PMID: 27397517

Davidson TJ, Kloosterman F, Wilson MA. 2009. Hippocampal replay of extended experience. *Neuron* **63**:497–507. DOI: https://doi.org/10.1016/j.neuron.2009.07.027, PMID: 19709631

DeLorey TM, Handforth A, Anagnostaras SG, Homanics GE, Minassian BA, Asatourian A, Fanselow MS, Delgado-Escueta A, Ellison GD, Olsen RW. 1998. Mice lacking the beta3 subunit of the GABAA receptor have the epilepsy phenotype and many of the behavioral characteristics of Angelman syndrome. *The Journal of Neuroscience* **18**:8505–8514. DOI: https://doi.org/10.1523/jneurosci.18-20-08505.1998, PMID: 9763493

Diba K, Buzsáki G. 2007. Forward and reverse hippocampal place-cell sequences during ripples. *Nature Neuroscience* **10**:1241–1242. DOI: https://doi.org/10.1038/nn1961, PMID: 17828259

Diekelmann S, Born J. 2010. The memory function of sleep. *Nature Reviews. Neuroscience* **11**:114–126. DOI: https://doi.org/10.1038/nrn2762, PMID: 20046194

Dudok B, Klein PM, Hwaun E, Lee BR, Yao Z, Fong O, Bowler JC, Terada S, Sparks FT, Szabo GG, Farrell JS, Berg J, Daigle TL, Tasic B, Dimidschstein J, Fishell G, Losonczy A, Zeng H, Soltesz I. 2021. Alternating sources of perisomatic inhibition during behavior. *Neuron* **109**:997–1012. DOI: https://doi.org/10.1016/j.neuron.2021.01.003, PMID: 33529646

Ego-Stengel V, Wilson MA. 2010. Disruption of ripple-associated hippocampal activity during rest impairs spatial learning in the rat. *Hippocampus* **20**:1–10. DOI: https://doi.org/10.1002/hipo.20707, PMID: 19816984

Einarsson EÖ, Nader K. 2012. Involvement of the anterior cingulate cortex in formation, consolidation, and reconsolidation of recent and remote contextual fear memory. *Learning & Memory* **19**:449–452. DOI: https://doi.org/10.1101/lm.027227.112, PMID: 22984282

Esparza J, Quintanilla JP, Cid E, Medeiros AC, Gallego JA, de la Prida LM. 2025. Cell-type-specific manifold analysis discloses independent geometric transformations in the hippocampal spatial code. *Neuron* **113**:1098–1109.. DOI: https://doi.org/10.1016/j.neuron.2025.01.022, PMID: 40015277

Fernández-Ruiz A, Oliva A, Fermino de Oliveira E, Rocha-Almeida F, Tingley D, Buzsáki G. 2019. Long-duration hippocampal sharp wave ripples improve memory. *Science* **364**:1082–1086. DOI: https://doi.org/10.1126/science.aax0758, PMID: 31197012

Foster DJ, Wilson MA. 2006. Reverse replay of behavioural sequences in hippocampal place cells during the awake state. *Nature* **440**:680–683. DOI: https://doi.org/10.1038/nature04587, PMID: 16474382

Frankland PW, Bontempi B, Talton LE, Kaczmarek L, Silva AJ. 2004. The involvement of the anterior cingulate cortex in remote contextual fear memory. *Science* **304**:881–883. DOI: https://doi.org/10.1126/science.1094804, PMID: 15131309

Freund TF, Gulyás AI, Acsády L, Görcs T, Tóth K. 1990. Serotonergic control of the hippocampus via local inhibitory interneurons. *PNAS* **87**:8501–8505. DOI: https://doi.org/10.1073/pnas.87.21.8501, PMID: 1700433

Gava GP, Lefèvre L, Broadbelt T, McHugh SB, Lopes-Dos-Santos V, Brizee D, Hartwich K, Sjoberg H, Perestenko PV, Toth R, Sharott A, Dupret D. 2024. Organizing the coactivity structure of the hippocampus from robust to flexible memory. *Science* **385**:1120–1127. DOI: https://doi.org/10.1126/science.adk9611, PMID: 39236189

Geiller T, Fattahi M, Choi JS, Royer S. 2017. Place cells are more strongly tied to landmarks in deep than in superficial CA1. *Nature Communications* **8**:14531. DOI: https://doi.org/10.1038/ncomms14531, PMID: 28218283

Girardeau G, Benchenane K, Wiener SI, Buzsáki G, Zugaro MB. 2009. Selective suppression of hippocampal ripples impairs spatial memory. *Nature Neuroscience* **12**:1222–1223. DOI: https://doi.org/10.1038/nn.2384, PMID: 19749750

Girardeau G, Inema I, Buzsáki G. 2017. Reactivations of emotional memory in the hippocampus-amygdala system during sleep. *Nature Neuroscience* **20**:1634–1642. DOI: https://doi.org/10.1038/nn.4637, PMID: 28892057

Giri B, Miyawaki H, Mizuseki K, Cheng S, Diba K. 2019. Hippocampal reactivation extends for several hours following novel experience. *The Journal of Neuroscience* **39**:866–875. DOI: https://doi.org/10.1523/JNEUROSCI.1950-18.2018, PMID: 30530857

Gridchyn I, Schoenenberger P, O'Neill J, Csicsvari J. 2020. Assembly-specific disruption of hippocampal replay leads to selective memory deficit. *Neuron* **106**:291–300. DOI: https://doi.org/10.1016/j.neuron.2020.01.021, PMID: 32070475

Grosmark AD, Buzsáki G. 2016. Diversity in neural firing dynamics supports both rigid and learned hippocampal sequences. *Science* **351**:1440–1443. DOI: https://doi.org/10.1126/science.aad1935, PMID: 27013730

Gulati T, Guo L, Ramanathan DS, Bodepudi A, Ganguly K. 2017. Neural reactivations during sleep determine network credit assignment. *Nature Neuroscience* **20**:1277–1284. DOI: https://doi.org/10.1038/nn.4601, PMID: 28692062

Halasy K, Miettinen R, Szabat E, Freund TF. 1992. GABAergic interneurons are the major postsynaptic targets of median raphe afferents in the rat dentate gyrus. *The European Journal of Neuroscience* **4**:144–153. DOI: https://doi.org/10.1111/j.1460-9568.1992.tb00861.x, PMID: 12106377

Hall AF, Wang DV. 2023. The two tales of hippocampal sharp-wave ripple content: The rigid and the plastic. *Progress in Neurobiology* **221**:102396. DOI: https://doi.org/10.1016/j.pneurobio.2022.102396, PMID: 36563928

Harris KD, Hirase H, Leinekugel X, Henze DA, Buzsáki G. 2001. Temporal interaction between single spikes and complex spike bursts in hippocampal pyramidal cells. *Neuron* **32**:141–149. DOI: https://doi.org/10.1016/s0896-6273(01)00447-0, PMID: 11604145

Harvey RE, Robinson HL, Liu C, Oliva A, Fernandez-Ruiz A. 2023. Hippocampo-cortical circuits for selective memory encoding, routing, and replay. *Neuron* **111**:2076–2090. DOI: https://doi.org/10.1016/j.neuron.2023.04.015, PMID: 37196658

Hefft S, Jonas P. 2005. Asynchronous GABA release generates long-lasting inhibition at a hippocampal interneuron-principal neuron synapse. *Nature Neuroscience* **8**:1319–1328. DOI: https://doi.org/10.1038/nn1542, PMID: 16158066

Huang W, Ikemoto S, Wang DV. 2022. Median raphe nonserotonergic neurons modulate hippocampal theta oscillations. *The Journal of Neuroscience* **42**:1987–1998. DOI: https://doi.org/10.1523/JNEUROSCI.1536-21.2022

Huang W, Hall AF, Kawalec N, Opalka AN, Liu J, Wang DV. 2026. Anterior cingulate cortex monitors action state and action content in complex associative learning. *eLife* **14**:e105774. DOI: https://doi.org/10.7554/eLife.105774.4, PMID: 39975180

Huelin Gorriz M, Takigawa M, Bendor D. 2023. The role of experience in prioritizing hippocampal replay. *Nature Communications* **14**:8157. DOI: https://doi.org/10.1038/s41467-023-43939-z, PMID: 38071221

Jackson J, Bland BH, Antle MC. 2009. Nonserotonergic projection neurons in the midbrain raphe nuclei contain the vesicular glutamate transporter VGLUT3. *Synapse* **63**:31–41. DOI: https://doi.org/10.1002/syn.20581, PMID: 18925658

Jadhav SP, Kemere C, German PW, Frank LM. 2012. Awake hippocampal sharp-wave ripples support spatial memory. *Science* **336**:1454–1458. DOI: https://doi.org/10.1126/science.1217230, PMID: 22555434

Jinde S, Zsiros V, Jiang Z, Nakao K, Pickel J, Kohno K, Belforte JE, Nakazawa K. 2012. Hilar mossy cell degeneration causes transient dentate granule cell hyperexcitability and impaired pattern separation. *Neuron* **76**:1189–1200. DOI: https://doi.org/10.1016/j.neuron.2012.10.036, PMID: 23259953

Karaba LA, Robinson HL, Harvey RE, Chen W, Fernandez-Ruiz A, Oliva A. 2024. A hippocampal circuit mechanism to balance memory reactivation during sleep. *Science* **385**:738–743. DOI: https://doi.org/10.1126/science.ado5708, PMID: 39146421

Karlsson MP, Frank LM. 2009. Awake replay of remote experiences in the hippocampus. *Nature Neuroscience* **12**:913–918. DOI: https://doi.org/10.1038/nn.2344, PMID: 19525943

Karson MA, Tang AH, Milner TA, Alger BE. 2009. Synaptic cross talk between perisomatic-targeting interneuron classes expressing cholecystokinin and parvalbumin in hippocampus. *The Journal of Neuroscience* **29**:4140–4154. DOI: https://doi.org/10.1523/JNEUROSCI.5264-08.2009, PMID: 19339609

Kim EJ, Pellman B, Kim JJ. 2015. Stress effects on the hippocampus: a critical review. *Learning & Memory* **22**:411–416. DOI: https://doi.org/10.1101/lm.037291.114, PMID: 26286651

Kim KR, Kim Y, Jeong HJ, Kang JS, Lee SH, Kim Y, Lee SH, Ho WK. 2021. Impaired pattern separation in Tg2576 mice is associated with hyperexcitable dentate gyrus caused by Kv4.1 downregulation. *Molecular Brain* **14**:62. DOI: https://doi.org/10.1186/s13041-021-00774-x, PMID: 33785038

Klausberger T, Marton LF, O'Neill J, Huck JHJ, Dalezios Y, Fuentealba P, Suen WY, Papp E, Kaneko T, Watanabe M, Csicsvari J, Somogyi P. 2005. Complementary roles of cholecystokinin- and parvalbumin-expressing GABAergic neurons in hippocampal network oscillations. *The Journal of Neuroscience* **25**:9782–9793. DOI: https://doi.org/10.1523/JNEUROSCI.3269-05.2005, PMID: 16237182

Klausberger T, Somogyi P. 2008. Neuronal diversity and temporal dynamics: the unity of hippocampal circuit operations. *Science* **321**:53–57. DOI: https://doi.org/10.1126/science.1149381, PMID: 18599766

Klinzing JG, Niethard N, Born J. 2019. Mechanisms of systems memory consolidation during sleep. *Nature Neuroscience* **22**:1598–1610. DOI: https://doi.org/10.1038/s41593-019-0467-3, PMID: 31451802

Lamotte G, Shouman K, Benarroch EE. 2021. Stress and central autonomic network. *Autonomic Neuroscience* **235**:102870. DOI: https://doi.org/10.1016/j.autneu.2021.102870, PMID: 34461325

Lee AK, Wilson MA. 2002. Memory of sequential experience in the hippocampus during slow wave sleep. *Neuron* **36**:1183–1194. DOI: https://doi.org/10.1016/s0896-6273(02)01096-6, PMID: 12495631

Lin L, Chen G, Xie K, Zaia KA, Zhang S, Tsien JZ. 2006. Large-scale neural ensemble recording in the brains of freely behaving mice. *Journal of Neuroscience Methods* **155**:28–38. DOI: https://doi.org/10.1016/j.jneumeth.2005.12.032, PMID: 16554093

Liu ZW, Faraguna U, Cirelli C, Tononi G, Gao XB. 2010. Direct evidence for wake-related increases and sleep-related decreases in synaptic strength in rodent cortex. *The Journal of Neuroscience* **30**:8671–8675. DOI: https://doi.org/10.1523/JNEUROSCI.1409-10.2010, PMID: 20573912

Liu J, Lin L, Wang DV. 2021. Representation of fear of heights by basolateral amygdala neurons. *The Journal of Neuroscience* **41**:1080–1091. DOI: https://doi.org/10.1523/JNEUROSCI.0483-20.2020, PMID: 33436527

Liu J, Goto A, Hayashi Y. 2024a. Time-window of offline long-term potentiation in anterior cingulate cortex during memory consolidation and recall. *Neuroscience Research* **212**:75–83. DOI: https://doi.org/10.1016/j.neures.2024.12.009, PMID: 40440255

Liu J, Hall AF, Wang DV. 2024b. Emerging many-to-one weighted mapping in hippocampus-amygdala network underlies memory formation. *Nature Communications* **15**:9248. DOI: https://doi.org/10.1038/s41467-024-53665-9, PMID: 39461946

Maris E, Oostenveld R. 2007. Nonparametric statistical testing of EEG- and MEG-data. *Journal of Neuroscience Methods* **164**:177–190. DOI: https://doi.org/10.1016/j.jneumeth.2007.03.024, PMID: 17517438

Masurkar AV, Srinivas KV, Brann DH, Warren R, Lowes DC, Siegelbaum SA. 2017. Medial and lateral entorhinal cortex differentially excite deep versus superficial CA1 pyramidal neurons. *Cell Reports* **18**:148–160. DOI: https://doi.org/10.1016/j.celrep.2016.12.012, PMID: 28052245

Miettinen R, Freund TF. 1992. Convergence and segregation of septal and median raphe inputs onto different subsets of hippocampal inhibitory interneurons. *Brain Research* **594**:263–272. DOI: https://doi.org/10.1016/0006-8993(92)91133-y, PMID: 1450951

Mizuseki K, Diba K, Pastalkova E, Buzsáki G. 2011. Hippocampal CA1 pyramidal cells form functionally distinct sublayers. *Nature Neuroscience* **14**:1174–1181. DOI: https://doi.org/10.1038/nn.2894, PMID: 21822270

Morales M, Bloom FE. 1997. The 5-HT3 receptor is present in different subpopulations of GABAergic neurons in the rat telencephalon. *The Journal of Neuroscience* **17**:3157–3167. DOI: https://doi.org/10.1523/JNEUROSCI.17-09-03157.1997, PMID: 9096150

Norimoto H, Makino K, Gao M, Shikano Y, Okamoto K, Ishikawa T, Sasaki T, Hioki H, Fujisawa S, Ikegaya Y. 2018. Hippocampal ripples down-regulate synapses. *Science* **359**:1524–1527. DOI: https://doi.org/10.1126/science.aao0702, PMID: 29439023

Oh SW, Harris JA, Ng L, Winslow B, Cain N, Mihalas S, Wang Q, Lau C, Kuan L, Henry AM, Mortrud MT, Ouellette B, Nguyen TN, Sorensen SA, Slaughterbeck CR, Wakeman W, Li Y, Feng D, Ho A, Nicholas E, et al. 2014. A mesoscale connectome of the mouse brain. *Nature* **508**:207–214. DOI: https://doi.org/10.1038/nature13186, PMID: 24695228

Oliva A, Fernández-Ruiz A, Leroy F, Siegelbaum SA. 2020. Hippocampal CA2 sharp-wave ripples reactivate and promote social memory. *Nature* **587**:264–269. DOI: https://doi.org/10.1038/s41586-020-2758-y, PMID: 32968277

Opalka AN, Huang WQ, Liu J, Liang H, Wang DV. 2020. Hippocampal ripple coordinates retrosplenial inhibitory neurons during slow-wave sleep. *Cell Reports* **30**:432–441. DOI: https://doi.org/10.1016/j.celrep.2019.12.038, PMID: 31940487

Papp EC, Hajos N, Acsády L, Freund TF. 1999. Medial septal and median raphe innervation of vasoactive intestinal polypeptide-containing interneurons in the hippocampus. *Neuroscience* **90**:369–382. DOI: https://doi.org/10.1016/s0306-4522(98)00455-2, PMID: 10215142

Petreanu L, Huber D, Sobczyk A, Svoboda K. 2007. Channelrhodopsin-2-assisted circuit mapping of long-range callosal projections. *Nature Neuroscience* **10**:663–668. DOI: https://doi.org/10.1038/nn1891, PMID: 17435752

Piñol RA, Bateman R, Mendelowitz D. 2012. Optogenetic approaches to characterize the long-range synaptic pathways from the hypothalamus to brain stem autonomic nuclei. *Journal of Neuroscience Methods* **210**:238–246. DOI: https://doi.org/10.1016/j.jneumeth.2012.07.022, PMID: 22890236

Raichle ME. 2015. The brain's default mode network. *Annual Review of Neuroscience* **38**:433–447. DOI: https://doi.org/10.1146/annurev-neuro-071013-014030, PMID: 25938726

Rajasethupathy P, Sankaran S, Marshel JH, Kim CK, Ferenczi E, Lee SY, Berndt A, Ramakrishnan C, Jaffe A, Lo M, Liston C, Deisseroth K. 2015. Projections from neocortex mediate top-down control of memory retrieval. *Nature* **526**:653–659. DOI: https://doi.org/10.1038/nature15389, PMID: 26436451

Ramanathan KR, Ressler RL, Jin J, Maren S. 2018. Nucleus reuniens is required for encoding and retrieving precise, hippocampal-dependent contextual fear memories in rats. *The Journal of Neuroscience* **38**:9925–9933. DOI: https://doi.org/10.1523/JNEUROSCI.1429-18.2018, PMID: 30282726

Ramanathan KR, Maren S. 2019. Nucleus reuniens mediates the extinction of contextual fear conditioning. *Behavioural Brain Research* **374**:112114. DOI: https://doi.org/10.1016/j.bbr.2019.112114, PMID: 31351844

Ratigan HC, Krishnan S, Smith S, Sheffield MEJ. 2023. A thalamic-hippocampal CA1 signal for contextual fear memory suppression, extinction, and discrimination. *Nature Communications* **14**:6758. DOI: https://doi.org/10.1038/s41467-023-42429-6, PMID: 37875465

Raven F, Aton SJ. 2021. The engram's dark horse: how interneurons regulate state-dependent memory processing and plasticity. *Frontiers in Neural Circuits* **15**:750541. DOI: https://doi.org/10.3389/fncir.2021.750541, PMID: 34588960

Rothschild G, Eban E, Frank LM. 2017. A cortical-hippocampal-cortical loop of information processing during memory consolidation. *Nature Neuroscience* **20**:251–259. DOI: https://doi.org/10.1038/nn.4457, PMID: 27941790

Senft RA, Freret ME, Sturrock N, Dymecki SM. 2021. Neurochemically and hodologically distinct ascending VGLUT3 versus serotonin subsystems comprise the r2-*Pet1* median raphe. *The Journal of Neuroscience* **41**:2581–2600. DOI: https://doi.org/10.1523/JNEUROSCI.1667-20.2021, PMID: 33547164

Sharif F, Tayebi B, Buzsáki G, Royer S, Fernandez-Ruiz A. 2021. Subcircuits of deep and superficial CA1 place cells support efficient spatial coding across heterogeneous environments. *Neuron* **109**:363–376. DOI: https://doi.org/10.1016/j.neuron.2020.10.034, PMID: 33217328

Shi W, Xue M, Wu F, Fan K, Chen QY, Xu F, Li XH, Bi GQ, Lu JS, Zhuo M. 2022. Whole-brain mapping of efferent projections of the anterior cingulate cortex in adult male mice. *Molecular Pain* **18**:17448069221094529. DOI: https://doi.org/10.1177/17448069221094529, PMID: 35354345

Silva BA, Astori S, Burns AM, Heiser H, van den Heuvel L, Santoni G, Martinez-Reza MF, Sandi C, Gräff J. 2021. A thalamo-amygdalar circuit underlying the extinction of remote fear memories. *Nature Neuroscience* **24**:964–974. DOI: https://doi.org/10.1038/s41593-021-00856-y, PMID: 34017129

Souza R, Bueno D, Lima LB, Muchon MJ, Gonçalves L, Donato J, Shammah-Lagnado SJ, Metzger M. 2022. Top-down projections of the prefrontal cortex to the ventral tegmental area, laterodorsal tegmental nucleus, and median raphe nucleus. *Brain Structure & Function* **227**:2465–2487. DOI: https://doi.org/10.1007/s00429-022-02538-2, PMID: 35869304

Squire LR, Genzel L, Wixted JT, Morris RG. 2015. Memory consolidation. *Cold Spring Harbor Perspectives in Biology* **7**:a021766. DOI: https://doi.org/10.1101/cshperspect.a021766, PMID: 26238360

Szőnyi A, Mayer MI, Cserép C, Takács VT, Watanabe M, Freund TF, Nyiri G. 2016. The ascending median raphe projections are mainly glutamatergic in the mouse forebrain. *Brain Structure & Function* **221**:735–751. DOI: https://doi.org/10.1007/s00429-014-0935-1, PMID: 25381463

Tononi G, Cirelli C. 2003. Sleep and synaptic homeostasis: a hypothesis. *Brain Research Bulletin* **62**:143–150. DOI: https://doi.org/10.1016/j.brainresbull.2003.09.004, PMID: 14638388

Tononi G, Cirelli C. 2006. Sleep function and synaptic homeostasis. *Sleep Medicine Reviews* **10**:49–62. DOI: https://doi.org/10.1016/j.smrv.2005.05.002, PMID: 16376591

Totah NKB, Jackson ME, Moghaddam B. 2013. Preparatory attention relies on dynamic interactions between prelimbic cortex and anterior cingulate cortex. *Cerebral Cortex* **23**:729–738. DOI: https://doi.org/10.1093/cercor/bhs057, PMID: 22419680

Turi GF, Li WK, Chavlis S, Pandi I, O'Hare J, Priestley JB, Grosmark AD, Liao Z, Ladow M, Zhang JF, Zemelman BV, Poirazi P, Losonczy A. 2019. Vasoactive intestinal polypeptide-expressing interneurons in the hippocampus support goal-oriented spatial learning. *Neuron* **101**:1150–1165.. DOI: https://doi.org/10.1016/j.neuron.2019.01.009, PMID: 30713030

Tzilivaki A, Tukker JJ, Maier N, Poirazi P, Sammons RP, Schmitz D. 2023. Hippocampal GABAergic interneurons and memory. *Neuron* **111**:3154–3175. DOI: https://doi.org/10.1016/j.neuron.2023.06.016, PMID: 37467748

Valero M, Cid E, Averkin RG, Aguilar J, Sanchez-Aguilera A, Viney TJ, Gomez-Dominguez D, Bellistri E, de la Prida LM. 2015. Determinants of different deep and superficial CA1 pyramidal cell dynamics during sharp-wave ripples. *Nature Neuroscience* **18**:1281–1290. DOI: https://doi.org/10.1038/nn.4074, PMID: 26214372

Valero M, Abad-Perez P, Gallardo A, Picco M, García-Hernandez R, Brotons J, Martínez-Félix A, Machold R, Rudy B, Buzsáki G. 2025. Cooperative actions of interneuron families support the hippocampal spatial code. *Science* **389**:eadv5638. DOI: https://doi.org/10.1126/science.adv5638, PMID: 40906860

Vancura B, Geiller T, Grosmark A, Zhao V, Losonczy A. 2023. Inhibitory control of sharp-wave ripple duration during learning in hippocampal recurrent networks. *Nature Neuroscience* **26**:788–797. DOI: https://doi.org/10.1038/s41593-023-01306-7, PMID: 37081295

Varga C, Oijala M, Lish J, Szabo GG, Bezaire M, Marchionni I, Golshani P, Soltesz I. 2014. Functional fission of parvalbumin interneuron classes during fast network events. *eLife* **3**:e04006. DOI: https://doi.org/10.7554/eLife.04006, PMID: 25375253

Wang J, Hasan MT, Seung HS. 2009. Laser-evoked synaptic transmission in cultured hippocampal neurons expressing channelrhodopsin-2 delivered by adeno-associated virus. *Journal of Neuroscience Methods* **183**:165–175. DOI: https://doi.org/10.1016/j.jneumeth.2009.06.024, PMID: 19560489

Wang DV, Yau HJ, Broker CJ, Tsou JH, Bonci A, Ikemoto S. 2015. Mesopontine median raphe regulates hippocampal ripple oscillation and memory consolidation. *Nature Neuroscience* **18**:728–735. DOI: https://doi.org/10.1038/nn.3998, PMID: 25867120

Wang DV, Ikemoto S. 2016. Coordinated interaction between hippocampal sharp-wave ripples and anterior cingulate unit activity. *The Journal of Neuroscience* **36**:10663–10672. DOI: https://doi.org/10.1523/JNEUROSCI.1042-16.2016, PMID: 27733616

Wang DV. 2026. Hall-and-wang-elife-2026. swh:1:rev:c91a265d13d36c8fc4017bdcd9fbf027e3197c4b. Software Heritage. https://archive.softwareheritage.org/swh:1:dir:0355b15c43412ab1caae86c3ed996f326b623512;origin=https://github.com/DVWangLab/Hall-and-Wang-eLife-2026;visit=swh:1:snp:6f8d12c6aa2a430457f936b4e980be38b29c08ac;anchor=swh:1:rev:c91a265d13d36c8fc4017bdcd9fbf027e3197c4b

Watson BO, Levenstein D, Greene JP, Gelinas JN, Buzsáki G. 2016. Network homeostasis and state dynamics of neocortical sleep. *Neuron* **90**:839–852. DOI: https://doi.org/10.1016/j.neuron.2016.03.036, PMID: 27133462

Wilson MA, McNaughton BL. 1994. Reactivation of hippocampal ensemble memories during sleep. *Science* **265**:676–679. DOI: https://doi.org/10.1126/science.8036517, PMID: 8036517

Xu W, Südhof TC. 2013. A neural circuit for memory specificity and generalization. *Science* **339**:1290–1295. DOI: https://doi.org/10.1126/science.1229534, PMID: 23493706